The Kinesin-3, Unc-104 Regulates Dendrite Morphogenesis and Synaptic Development in *Drosophila*

Jeannine V. Kern,*,† Yao V. Zhang,*,†,‡ Stella Kramer,† Jay E. Brenman,§ and Tobias M. Rasse*,†

*Junior Research Group Synaptic Plasticity and †Department of Cellular Neurology, Hertie Institute for Clinical Brain Research, University of Tübingen, 72076 Tübingen, Germany, ‡Graduate School of Cellular and Molecular Neuroscience, University of Tübingen, 72074 Tübingen, Germany, and §Neuroscience Center, University of North Carolina School of Medicine, Chapel Hill, North Carolina 27599

ABSTRACT Kinesin-based transport is important for synaptogenesis, neuroplasticity, and maintaining synaptic function. In an anatomical screen of neurodevelopmental mutants, we identified the exchange of a conserved residue (R561H) in the forkhead-associated domain of the kinesin-3 family member Unc-104/KIF1A as the genetic cause for defects in synaptic terminal- and dendrite morphogenesis. Previous structure-based analysis suggested that the corresponding residue in KIF1A might be involved in stabilizing the activated state of kinesin-3 dimers. Herein we provide the first *in vivo* evidence for the functional importance of R561. The R561H allele (*unc-104^{bris}*) is not embryonic lethal, which allowed us to investigate consequences of disturbed Unc-104 function on postembryonic synapse development and larval behavior. We demonstrate that Unc-104 regulates the reliable apposition of active zones and postsynaptic densities, possibly by controlling site-specific delivery of its cargo. Next, we identified a role for Unc-104 in restraining neuromuscular junction growth and coordinating dendrite branch morphogenesis, suggesting that Unc-104 is also involved in dendritic transport. Mutations in *KIF1A/unc-104* have been associated with hereditary spastic paraplegia and hereditary sensory and autonomic neuropathy type 2. However, we did not observe synapse retraction or dystonic posterior paralysis. Overall, our study demonstrates the specificity of defects caused by selective impairments of distinct molecular motors and highlights the critical importance of Unc-104 for the maturation of neuronal structures during embryonic development, larval synaptic terminal outgrowth, and dendrite morphogenesis.

SYNAPSE formation and maturation depend on kinesin-based fast anterograde transport (Hirokawa *et al.* 2010; Kondo *et al.* 2012; van den Berg and Hoogenraad 2012). Key synaptic components such as synaptic vesicle precursors (Hall and Hedgecock 1991), mitochondria (Nangaku *et al.* 1994), piccolo-bassoon transport vesicles (Cai *et al.* 2007), and RNA–protein complexes (Ohashi *et al.* 2002) are transported by members of the kinesin-1 or kinesin-3 families (for review see Hirokawa and Noda 2008). To date, only a limited understanding of the mechanisms underlying cargo specificity and the dynamic regulation of cargo–motor complexes has emerged. In particular, factors that mediate motor activation and cargo binding and release remain to be elucidated (for review see Verhey and Hammond 2009; Verhey *et al.* 2011).

In an anatomical screen examining mutants that might be involved in synaptogenesis, we identified a weak hypomorphic mutation (R561H) in the kinesin-3 family member Unc-104. *KIF1A/unc-104* has been implicated in hereditary spastic paraplegia (HSP) (Erlich *et al.* 2011; Klebe *et al.* 2012) and hereditary sensory and autonomic neuropathy type 2 (Riviere *et al.* 2011). The R561H allele (*unc-104^{bris}*) is not embryonic lethal allowing for detailed larval behavioral analysis. No synapse retraction or dystonic posterior paralysis, as described for the HSP type 10 *Drosophila* model, in which kinesin-1-based axonal transport is disturbed (Fuger *et al.* 2012), were observed. Rather, the observed defects were mostly neurodevelopmental.

The affected arginine residue (R561) localizes to the β11-loop of the forkhead-associated (FHA) domain of Unc-104.

doi: 10.1534/genetics.113.151639
Manuscript received March 26, 2013; accepted for publication June 6, 2013
Available freely online through the author-supported open access option.
Supporting information is available online at http://www.genetics.org/lookup/suppl/doi:10.1534/genetics.113.151639/-/DC1.
Corresponding author: Junior Research Group Synaptic Plasticity, Hertie Institute for Clinical Brain Research, University of Tübingen, Otfried Müller Strasse 25, 72076 Tübingen, Germany. E-mail: tobias.rasse@uni-tuebingen.de

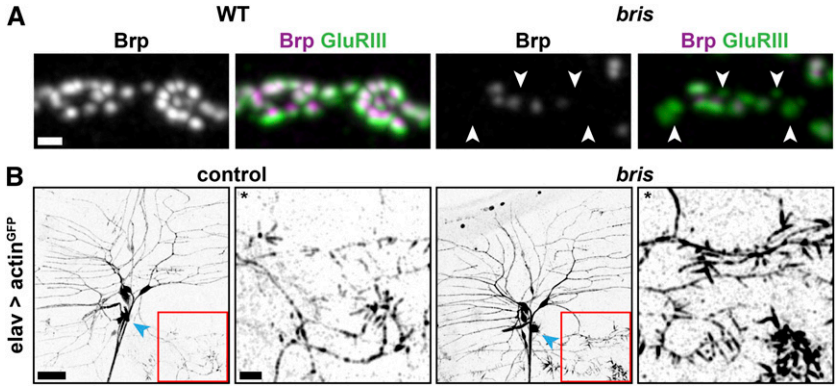

Figure 1 *Bristly* (*bris*) mutants are characterized by defects in synaptogenesis and dendritic filopodia formation. (A) Confocal immunofluorescence images showing several synaptic boutons at NMJ 4 of mid-third instar *Drosophila* larvae. Wild-type and *bris* larvae were stained for glutamate receptor III (GluRIII, green) and Bruchpilot (Brp, gray and magenta). Many PSDs are unapposed by a presynaptic Brp puncta (arrowheads) in *bris* larvae. Bar, 1 μm. (B) While dendritic branching of the neuron ddaA (cell body, blue arrowhead) is unaffected, greatly increased filopodia formation at distal secondary branches is detected in *bris* third-instar larvae. Bar, 20 μm. *For visualization of secondary branches, brightness and contrast were adjusted in both enlargements. Bar, 10 μm.

Structure-based analysis suggests that interaction of the corresponding residue (R583) in human KIF1A with the E499 residue located in the β1/β2-loop might stabilize kinesin-3 dimers (Huo *et al.* 2012). The functional relevance of the interaction has not yet been elucidated. Here, we employed larvae as a model to investigate the functional importance of Unc-104 during larval development and to characterize the effects of disrupting the proposed electrostatic interaction between the β11- and the β1/β2-loop *in vivo*.

We show that R561 is important for kinesin-3 function and provide evidence that Unc-104 critically restricts neuromuscular junction (NMJ) growth during larval development. Moreover, Unc-104 is essential for the reliable apposition of active zones (AZs) and postsynaptic densities (PSDs) and controls dendrite branch morphogenesis. In addition to previously described roles (Pack-Chung *et al.* 2007; Barkus *et al.* 2008), these novel functions demonstrate that Unc-104 orchestrates synapse formation and maturation at the NMJ during embryonic and larval development and also regulates dendrite morphogenesis.

Materials and Methods

Fly stocks

Flies were raised on standard medium at 25° unless otherwise noted. The following fly strains were used in this study: *unc-104*^{d11204} (Thibault *et al.* 2004), *Df(2R)Exel 7145* (O'Farrell *et al.* 2008), *Df(2R)Exel 6064* (Parks *et al.* 2004), *Df(2R)ED 3181*, *elav*^{C155}*-Gal4*, *D42-Gal4*, and *UAS-actin*^{GFP}. *UAS-unc-104*^{mCherry} was obtained from Thomas Schwarz (Harvard University, Cambridge, MA). Transgenic RNAi stocks were obtained from the Vienna *Drosophila* RNAi Center (Dietzl *et al.* 2007). *UAS-Brp* and *UAS-Brp-RNAi* stocks were obtained from Stephan Sigrist (Freie Universität Berlin, Germany).

Fly strains were obtained from the Bloomington Stock Center unless otherwise noted.

Immunohistochemistry

For preparation of larval fillets, third instar larvae were dissected essentially as previously described (Qin *et al.* 2005). In brief, larvae were gently stretched and immobilized on a dissection plate with the dorsal midline of the larvae facing upward. Insect pins were positioned at the anterior and posterior end of the larvae. After applying a drop of ice-cold hemolymph-like saline solution, the larvae were cut open along the dorsal midline. The epidermis was stretched and fixed using insect pins. Internal organs were removed using forceps. Care was taken to avoid damaging the body wall muscles and the central nervous system. Next, larvae were fixed (4% paraformaldehyde in phosphate buffered saline, PBS), blocked (PBS, 5% normal goat serum, 0.05% Triton X-100), and stained with primary (4°, overnight) and secondary (2 h at room temperature) antibodies essentially as previously described (Qin *et al.* 2005).

The peptide (PRRSLDKSLDRTPKS) was used to generate and affinity purify the rabbit anti-GluRIII antibody. The purified antibody was used at a 1:1000 dilution. The following primary antibodies, obtained from the Developmental Studies Hybridoma Bank, were used at the concentrations indicated: Bruchpilot (nc82) 1:100 and Dlg (4F3) 1:50. VGlut (1:1000) was obtained from Hermann Aberle (Mahr and Aberle 2006), and Unc-104/Imac (1:1000) from Thomas Schwarz (Pack-Chung *et al.* 2007). Horseradish peroxidase (HRP)-Cy3 (1:500) and HRP-Cy5 (1:500) were obtained from Dianova. The fluorescence-labeled secondary antibodies were from Invitrogen, Molecular Probes, or from Fluka/Sigma.

Embryo collection and fixation

Embryos were collected on apple juice plates at 25°. At 16.5 h after egg laying (AEL), embryos were prepared for confocal microscopy as previously described (Mahr and Aberle 2006).

Analysis of sensory neurons

To analyze the dendritic branches in body-wall sensory neurons, larvae were killed by immersing them for 2–4 s in 65° water. Next, larvae were mounted in a chamber originally designed for *in vivo* imaging and imaged within 15 min on a Zeiss LSM 710 confocal microscope. Details on the construction of the chamber and larvae mounting have been previously described (Fuger *et al.* 2007; Zhang *et al.* 2010).

Imaging and analysis

Whole larvae or larval fillets were imaged on a Zeiss LSM 710 confocal microscope, equipped with 405, 440, 488, 514, 561,

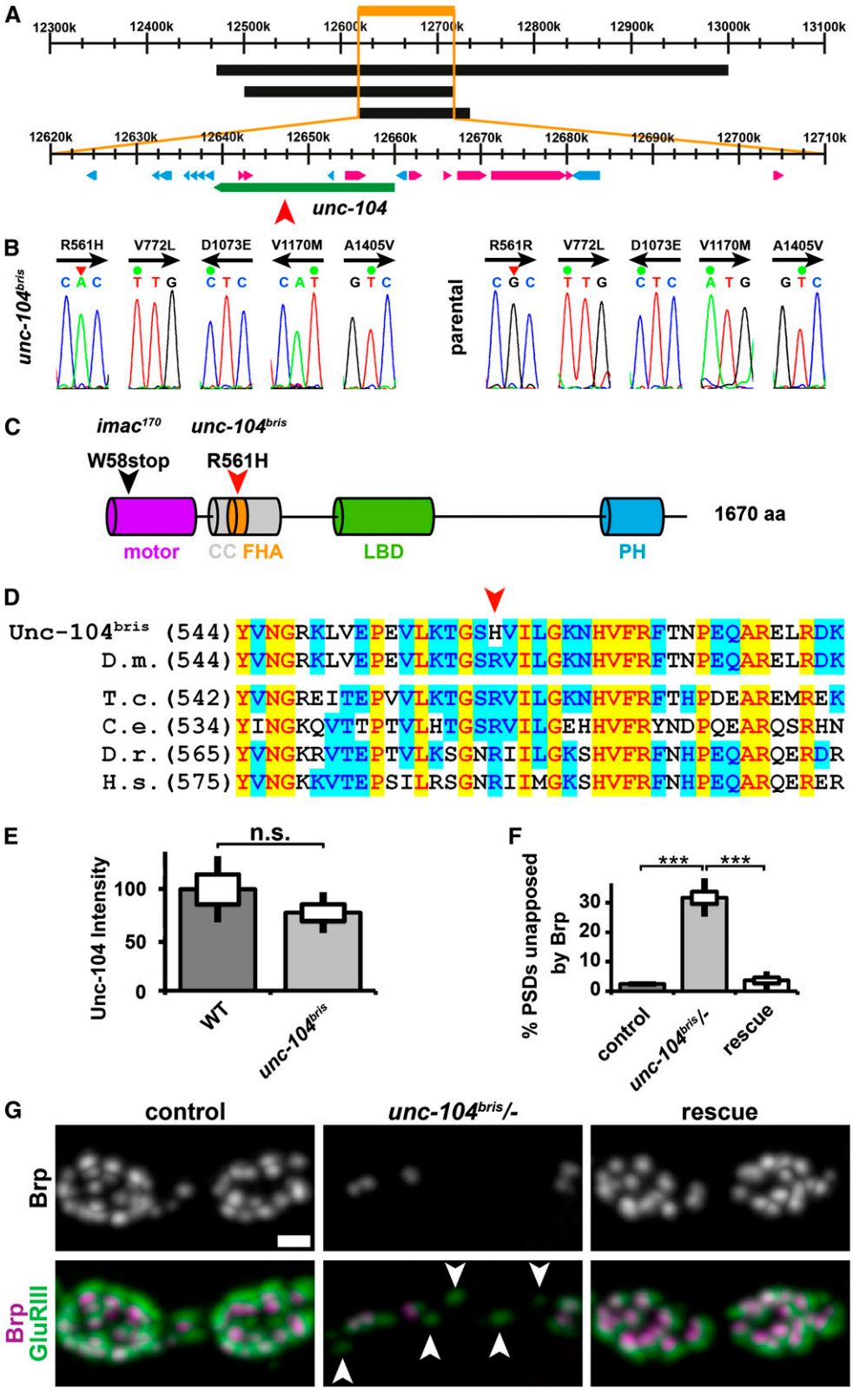

Figure 2 *bristly* is an allele of the neuronal kinesin-3 family member *unc-104/KIF1A*. (A) Schematic of the *unc-104* gene locus. Numbers indicate the chromosomal base pair position. Three overlapping deficiencies denoted as black boxes (from top to bottom Df (2R): Exel7145, Exel 6064, ED 3181) failed to complement the *bris* locus. The three deficiencies overlap at position (2R) 12.618.999–12.714.156 (orange) of the *Drosophila* genome. The XP insertion *unc-104*^{d11204} (red arrowhead) failed to complement *bris*. Unc-104 is denoted as a green box; other genes in the identified region are shown in blue or pink. (B) Five alterations from the *unc-104* reference sequence deposited at Flybase (Entrez GeneID: 36876, FBgn0034155) could be identified. Four of these mutations (V722L, D1073E, V1170M, and A1450V) represent likely polymorphisms because they were present in the parental strain used to perform the mutagenesis (left panel, *unc-104*^{bris} and right panel, parental strain). The original sequencing reads are shown. Arrow indicates the sequenced DNA strand. (C) Predicted domain structure of *unc-104* and locations of selected mutations. R561H localizes to a conserved residue in the FHA domain of *unc-104*. Motor domain, purple; coiled coil-rich region, gray; FHA domain, orange; liprin binding domain (LBD), green; and PH domain, blue. (D) Alignment of Unc-104 in various species [*Drosophila melanogaster* (D.m.), *Tribolium castaneum* (T.c.), *Caenorhabditis elegans* (C. e.), *Danio rerio* (D.r.), and *Homo sapiens* (H.s.)]. The mutated R561 residue (red arrowhead) is conserved across all species examined. (E) Unc-104 abundance is not significantly reduced in ventral nerve cords of *unc-104*^{bris} larvae. (F) Percentage of PSDs unapposed by Brp were quantified in NMJ 4, segment A2 of mid-third instar *Drosophila* larvae of the following genotypes: *elav-Gal4/+;;UAS-unc-104*^{mCherry}*/+* (control), *unc-104*^{bris}*/−; UAS-unc-104*^{mCherry}*/+* (*unc-104*^{bris}*/−*), and *elav-Gal4/+;unc-104*^{bris}*/−;UAS-unc-104*^{mCherry}*/+* (rescue). The standard error of the mean (SEM) is shown as a box, the standard deviation (SD) as a black line. ***$P < 0.001$. (G) Synaptic boutons at NMJ 4 of mid-third instar *Drosophila* larvae stained for GluRIII (green) and Brp (gray and magenta). Panneuronal expression of *unc-104*^{mCherry} rescues defects in the apposition of AZs and PSDs. Arrowheads point at PSDs unapposed by a Brp-positive AZ. Bar, 1 μm.

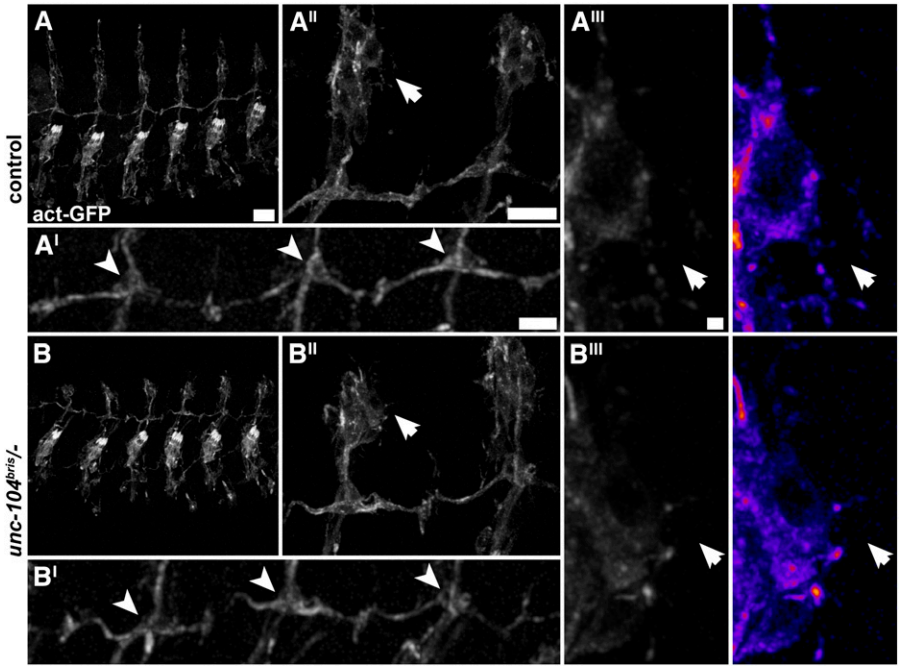

Figure 3 Dendrite morphology is unchanged in *unc-104^{bris}*/− embryos at 16.5 h AEL. (A and B) Confocal images of sensory neurons in embryos that express *UAS-actin^{GFP}* panneuronally (*elav-Gal4/+;;UAS-actin^{GFP}/+* [control] and *unc-104^{bris}/−;UAS-actin^{GFP}/+* [*unc-104^{bris}/−]). (A and B) No morphological alterations were observed in *unc-104^{bris}/−* embryos. (A′ and B′) The axonal or dendritic morphology of bipolar (arrowheads) or dendritic arborization neurons (A′′,A′′′,B′′, and B′′′; arrows) is indistinguishable between *unc-104^{bris}/−* and control embryos. Bars: A, 20 μm; A′ and A′′, 10 μm; A′′′, 1 μm.

and 633 laser lines and a ConfoCor 3 scanhead using a 40× Plan-Apochromat 1.3 N.A. or a 63× Plan-Apochromat 1.4 N.A. objective. Unless otherwise specified, the images were obtained using photomultiplier tube (PMT) detection. If fluorescence intensity was low, the sample was imaged using avalanche photodiode (APD) detection. Unless otherwise specified, the voxel dimensions (x/y/z) for NMJs were 100 × 100 × 500 nm and for ventral nerve cords, 300 × 300 × 1000 nm.

Embryonic or larval sensory neurons were recorded with the following voxel sizes: embryonic sensory neurons shown in Figure 3, A, A′, B, and B′: 346 × 346 × 750 nm; embryonic sensory neurons shown in Figure 3, A′′, A′′′, B′′, B′′′: 100 × 100 × 500 nm; and larval sensory neurons: 520 × 520 × 750 nm. Images were scaled by a factor of 2, and Gaussian blur filtering was applied (pixel radius = 2). Gamma values were adjusted for illustrational purposes to 0.75. For qualitative comparison of morphology, each genotype was imaged at the maximum level of brightness while avoiding saturation. For quantitative comparisons of intensities, common settings were chosen to avoid oversaturation in any of the genotypes. Image processing was performed using ImageJ v. 1.40g.

The length of NMJs is the sum of the length of all branches. NMJ area was determined by measuring the HRP-positive area. The HRP signal was first rescaled by a factor of 2 and then filtered (Gaussian blur, pixel radius: 2) and z projected (maximum intensity projection). Next, a dynamic threshold was applied to the HRP signal to create a mask that defines the NMJ size. This dynamic threshold is constant within a given genotype, but might differ between genotypes. It was set to 40% of the mean HRP intensity measured in a given genotype. Bouton numbers were counted manually.

NMJ size and bouton number were normalized to the square of the muscle length, and NMJ length was normalized to the muscle length. Only muscles within the size range: 180–350 μm were included in the normalization. Nonnormalized NMJ length and size, as well as boutons per NMJ and muscle length are shown for comparison in Supporting Information, Figure S1, A–D.

Locomotion analysis

All solutions used to wash larvae were at room temperature. Behavioral assays were performed at 25° at 70% humidity.

For qualitative analysis of larval behavior, single larvae were placed on a thin slice of apple juice agar. Dystonic posterior paralysis behavior was scored visually. The animals were recorded at a frame rate of 30 fps for 5 min using a DCM510 camera (ScopeTek, P. R. China) integrated in a custom-built stereomicroscope. Videos were converted using Prism Video Converter, v. 1.61 (NCH Software, Canberra, Australia) and further processed using VirtualDub 1.9.10 and ImageJ v. 1.40g. Size is the main determinant of larval locomotion speed (Fuger *et al.* 2012). We thus analyzed size-matched, rather than stage- or age-matched larvae that might be slower due to delayed development and smaller size.

For quantitative analysis, up to 200 larvae were recovered from food, dispersed in 15% sucrose solution, rinsed with tap water, and stored on a temperature- and humidity-controlled agar plate for 45 min. Next, the larvae were recorded on a 15 × 15 cm agar plate for 10 min. Locomotion speed and size of larvae were analyzed with the custom-built software Animaltracer (Fuger *et al.* 2012). Larvae that touched each other were excluded from analysis. Larvae whose velocity was <10% of average velocity of the respective genotype were excluded from analysis. This selection criterion prevented the erroneous inclusion of dead larvae or debris in the dataset. Average locomotion speed was separately calculated for each size group. A minimum of six experiments per genotype were analyzed.

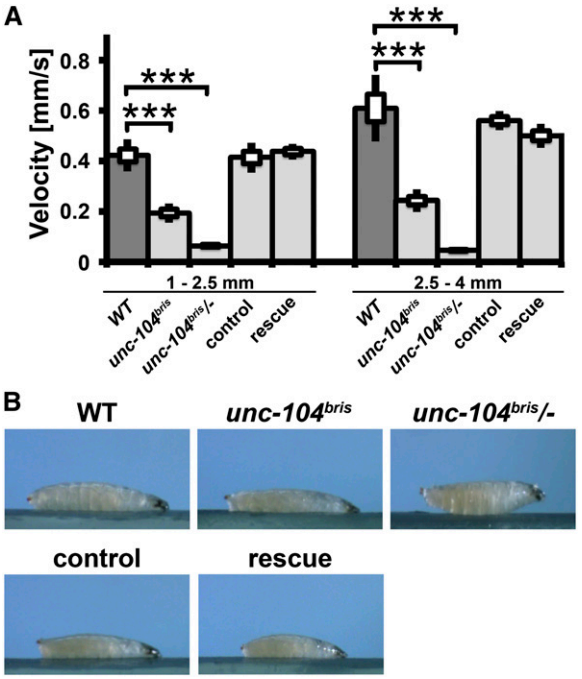

Figure 4 Impaired larval locomotor activity in *unc-104*^{bris} larvae. (A) *unc-104*^{bris} larvae are slower than wild-type larvae. *unc-104*^{bris}/− larvae are largely immobile and die in the late third instar stage. (B) Larvae in the act of crawling. No dystonic posterior paralysis is observed. *unc-104*^{bris}/− larvae display a body posture defect that can be rescued by panneuronal expression of *unc-104*^{mCherry}. The SEM is shown as a box, the SD as a black line. ***$P < 0.001$.

For all further statistical analysis, "*n*" was defined as the number of experiments.

Statistical analysis

Statistical tests were performed with PAST software (http://folk.uio.no/ohammer/past/index.html) unless otherwise noted. Sample errors are given as standard deviation (SD) and standard error of the mean (SEM). Statistical tests used in this study are documented in Table S1. The following alpha levels were used for all tests: *$P < 0.05$, **$P < 0.01$, and ***$P < 0.001$.

Genetic screen

To score for defects in synapse formation and maintenance, immunostainings of type I boutons of *Drosophila* larvae were analyzed. At the investigated NMJ (NMJ 4, segment A3) typically >95% of all PSDs are apposed by mature AZs. We used the cytomatrix of the AZ protein Bruchpilot (Brp) (Kittel *et al.* 2006) and the glutamate receptor subunit III (GluRIII) (Marrus *et al.* 2004) as molecular marker for AZs and PSDs, respectively. Mutant strains in which a significant number of unapposed PSDs or AZs were detected upon visual inspection were isolated for further analysis.

Mapping of bristly

To map the *bris* gene mutation, the original stock was outcrossed to a control *Drosophila* strain (*white*^{1118}) for three generations. Next, we identified three overlapping deficiencies (Thibault *et al.* 2004; Ryder *et al.* 2007) (Df(2R): Exel 7145, Exel 6064, and ED 3181) that failed to complement the *bristly* locus. These deficiencies overlap at position (2R) 12.618.999–12.714.156 of the *Drosophila* genome. The same area was identified utilizing recombination-based mapping with molecularly defined *P*-element insertions (Zhai *et al.* 2003). Next, we tested mutations that affect candidate genes in the identified region.

Results

bristly is an allele of the neuronal kinesin-3 family member unc-104/KIF1A

Although cytoskeletal structure, membrane protein sorting, and protein targeting mechanisms can be distinct between dendrites and axons, there are a considerable number of proteins important for both axonal and dendritic morphogenesis (Gao *et al.* 1999). We therefore decided to systematically screen mutants with abnormal dendrite morphogenesis for defects in synapse formation and maintenance. We selected *bristly* (*bris*) larvae, in which 17% of all PSDs at NMJs 4 are not apposed by a Brp-positive AZ for further characterization (Figure 1A).

bris was originally isolated due to enhanced filopodia formation at the tip of the neuron ddaA (Figure 1B and Medina *et al.* 2006) but did not show obvious defects in dendritic branching (Figure 1B and Medina *et al.* 2006). The XP insertion *unc-104*^{d11204} in the kinesin-3 *unc-104* failed to complement the *bristly* mutation (Figure 2A, red arrowhead). Sequencing revealed five predicted amino acid changes compared to the referral sequence (Entrez Gene ID: 36876, FBgn0034155): R561H, V722L, D1073E, V1170M, and A1450V (Figure 2B). In contrast to the other four amino acid substitutions, the R561H mutation is absent in the parental strain used to perform the mutagenesis. Except for R561H, the other amino acid substitutions are predicted conservative substitutions. Hence, we concluded that four of the discrepancies from the database sequence (V722L, D1073E, V1170M, and A1450V) are naturally occurring polymorphisms (Figure 2B), while R561H is responsible for the observed phenotype. The original sequences are available in File S1. R561 is a highly conserved residue in the FHA domain (Figure 2, C and D), which is considered potentially important for dimerization and activation of kinesin-3 motors (Huo *et al.* 2012).

Previously described *unc-104* null mutants (*unc-104*^{170}/Df(2R)DAlk21) are embryonic lethal (Pack-Chung *et al.* 2007); however, homozygous *unc-104*^{bris} larvae or transheterozygous (*unc-104*^{bris}/*unc-104*^{d11204} and *unc-104*^{bris}/*unc-104*^{170}) larvae die in the third instar larval stage. This new hypomorphic mutation therefore provides a powerful tool to investigate later neuronal processes that might depend on Unc-104/KIF1A. R561H does not adversely affect the stability of Unc-104^{bris} as quantified by immunostaining in ventral nerve cords (Figure 2E). Panneuronal expression of an mCherry-tagged *unc-104* cDNA construct is sufficient to

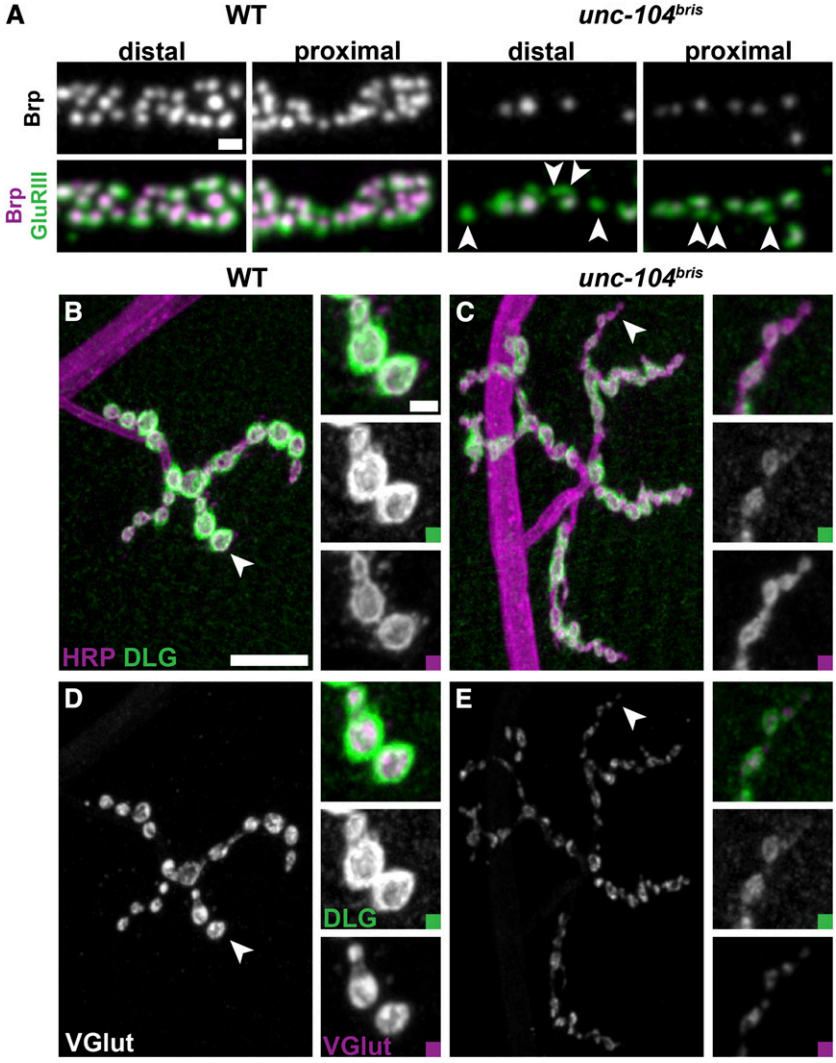

Figure 5 No synapse retraction observed in *unc-104^{bris}* larvae. (A) Proximal and distal synaptic boutons at NMJ 4 of mid-third instar *Drosophila* larvae stained for GluRIII (green) and Brp (gray and magenta). Unapposed PSDs (arrowheads) localize to proximal and distal boutons in *unc-104^{bris}* larvae. Bar, 1 μm. (B–E) NMJ 4, segment A2 or A3 of mid-third instar *Drosophila* wild-type (B and D) and *unc-104^{bris}* (C and E) larvae were stained for the membrane marker HRP (B and C; magenta), the postsynaptic scaffolding protein Discs-large (Dlg) (B–E, green), and the vesicular glutamate transporter (VGlut) (D and E, gray and magenta). The presence of organized postsynaptic Dlg staining unapposed by presynaptic structures is indicative of synapse retraction, which typically occurs at distal boutons (arrowheads). No synapse retraction was observed in *unc-104^{bris}* larvae. Bars, 10 μm and 2 μm (magnified panel).

rescue transheterozygous *unc-104^{bris}/unc-104^{d11204}* larvae (from now on referred to as: *unc-104^{bris}/−*) to full viability. Panneuronal expression of *unc-104^{mCherry}* using elav-Gal4 is also sufficient to rescue defects in the reliable apposition of AZs and PSDs in *unc-104^{bris}/−* larvae (Figure 2, F and G). We thus concluded that observed phenotypes are specifically caused by the loss of Unc-104 function.

Dendrite morphogenesis

We next sought to address the cellular basis for the observed dendritic morphology alterations. Dendritic morphology is continuously refined by multiple interrelated pathways controlling outgrowth, branching, guidance, and pruning (Corty *et al.* 2009). For simplicity, we only differentiated between initial neurite outgrowth in the developing embryo and dendrite maturation, which includes morphological changes during later outgrowth, branching, guidance, and pruning.

unc-104 expression is first detectable in stage 11 embryos (Pack-Chung *et al.* 2007). At 14 h AEL, homozygous *unc-104^{116}* null mutant embryos displayed abnormal axonal growth cone morphology (Pack-Chung *et al.* 2007). We scored defects in initial sensory neurite outgrowth in mid-stage 16 embryos (16.5 h AEL), in which *unc-104^{bris}* has been expressed for roughly 10 h to allow for the manifestation of defects. Sensory neurons were visualized by panneuronal expression of *UAS-actin^{GFP}*. No gross morphological alterations of the peripheral sensory neuron system were observed in *unc-104^{bris}/−* embryos (Figure 3, A and B). Dorsal dendrite extension was nearly completed at 16.5 h AEL both in *unc-104^{bris}/−* and control embryos. No obvious alterations in axonal or dendritic morphology of bipolar neurons (Figure 3, A′ and B′; arrowheads) or dendritic arborization neurons (Figure 3, A′′, A′′′, B′′, and B′′′; arrows) were observed. Hence, we concluded that the morphological defects observed in L3 larvae (Figure 1B and Medina *et al.* 2006) were caused by impairments in dendrite maturation.

unc-104^{bris} larvae are characterized by impaired larval locomotion

Mutations in the human *unc-104* homolog *KIF1A* cause HSP (Erlich *et al.* 2011; Klebe *et al.* 2012) or hereditary sensory and autonomic neuropathy type 2 (Riviere *et al.* 2011). We

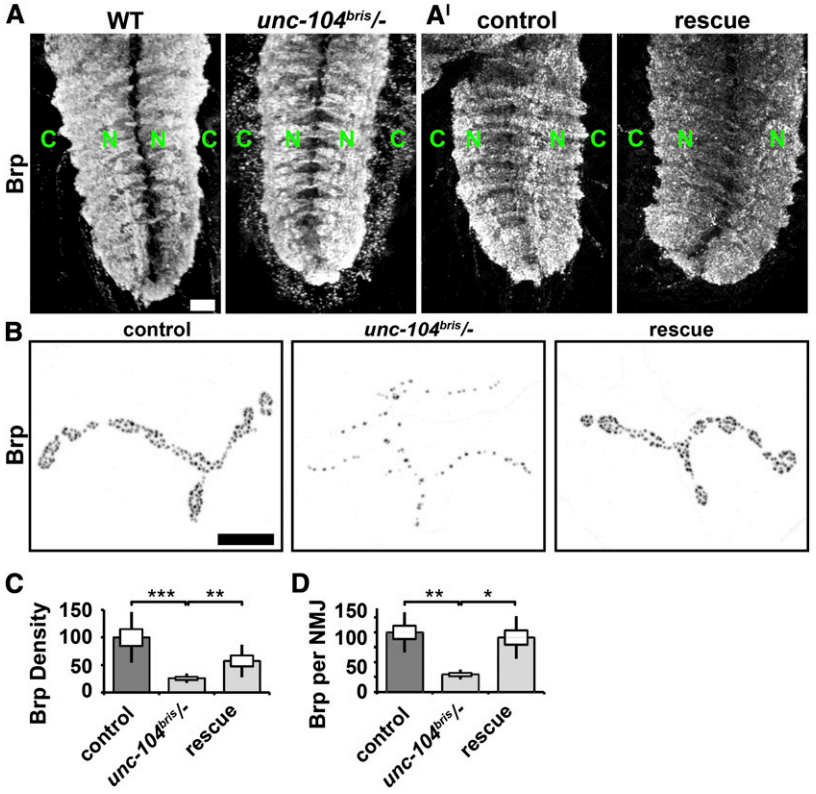

Figure 6 Axonal transport of Brp is impaired in *unc-104^{bris}*/− larvae. (A and A′) Ventral nerve cords of mid-third instar *Drosophila* larvae were stained for Brp, which is concentrated in the neuropil region (green N) of wild-type larvae, but is found in the cortex of *unc-104^{bris}*/− larvae (green C). (A′) Panneuronal expression of Unc-104^{mCherry} (rescue) restores Brp neuropil localization in *unc-104^{bris}*/− larvae. Bar, 20 μm. (B) NMJ 4, segment A2 of mid-third instar *Drosophila* larvae of the following genotypes: *elav-Gal4/+;;UAS-unc-104^{mCherry}/+* (control), *unc-104^{bris}/−;UAS-unc-104^{mCherry}/+* (*unc-104^{bris}*/−), or *elav-Gal4/+;unc-104^{bris}/−;UAS-unc-104^{mCherry}/+* (rescue) were stained for Brp. Bar, 10 μm. (C) Brp density and (D) Brp abundance per NMJ are reduced in *unc-104^{bris}*/− larvae compared to control larvae and *unc-104^{bris}*/− larvae expressing *unc-104^{mCherry}*. The SEM is shown as a box, the SD as a black line. $*P < 0.05$, $**P < 0.01$, $***P < 0.001$.

sought to use *unc-104^{bris}* larvae as a model for the cellular consequences of a moderate loss of *unc-104* function that might be relevant in the context of HSP.

HSP is characterized by progressive spasticity and paralysis of the lower extremities. The selective vulnerability of long motoneuron-axons in the corticospinal tract is an important cellular hallmark of HSP. For HSP type 10 (HSP10) caused by autosomal dominant mutations in *KIF5A/khc*, this axon length-dependent vulnerability of motoneurons could be replicated in *Drosophila* larvae by ectopic expression of mutant *khc* in the wild-type background (HSP10-model larvae) (Fuger *et al.* 2012). A selective vulnerability of posterior segments was evident by exacerbated morphological defects at synaptic terminals and dystonic posterior paralysis (tail-flip phenotype) (Fuger *et al.* 2012).

Neither homozygous *unc-104^{bris}* larvae nor transheterozygous *unc-104^{bris}*/− larvae displayed dystonic posterior paralysis, indicating that these larvae suffered from impairments distinct from those caused by impaired Khc function (Hurd and Saxton 1996; Fuger *et al.* 2012).

HSP10 model larvae displayed a size-dependent reduction in larval locomotion speed that is most pronounced in large larvae (Fuger *et al.* 2012). Semiautomated analysis using the custom-built algorithm Animaltracer (Fuger *et al.* 2012) revealed that both small and large homozygous *unc-104^{bris}* larvae are slower than control larvae, whereby the degree of impairment in larval locomotion relative to control larvae is independent of larval size (for larval length 1–2.5 mm, wt: 0.42 ± 0.03 mm/s, $n = 6$; *unc-104^{bris}*: 0.19 ± 0.01 mm/s, $n = 7$ and for larval length 2.5–4 mm, wt: 0.61 ± 0.05 mm/s, $n = 6$; *unc-104^{bris}*: 0.24 ± 0.02 mm/s, $n = 8$). The genetically more impaired transheterozygous *unc-104^{bris}*/− larvae were almost paralyzed (Figure 4A) and displayed a body posture defect (Figure 4B).

Comparative behavioral analysis revealed that impairments in anterograde molecular motor function caused by either ectopic overexpression of dominant-negative *khc* constructs or the hypomorphic *unc-104^{bris}* allele led to distinct behavioral defects. Those caused by the *unc-104^{bris}* allele were likely neurodevelopmental and not neurodegenerative in nature, possibly due to the impaired maturation of a subset of synapses.

Synaptic terminals in unc-104^{bris} larvae are not subject to neurodegeneration

KIF1A has been shown to be important for hippocampal synaptogenesis and synaptic bouton formation (Hirokawa *et al.* 2010). During *Drosophila* synaptogenesis, Brp is reliably recruited to nascent AZs within a few hours following new PSD formation (Rasse *et al.* 2005). This matching of PSDs and AZs is disturbed in *unc-104^{bris}*/− larvae. Defects in apposition might occur due to (i) presynaptic nerve retraction, (ii) rate limiting abundance of Brp, (iii) delivery of Brp to extrasynaptic sites, or (iv) disturbances in the molecular mechanism that allocate AZ components such that all synapses receive at least the minimal amount necessary to assemble a fully functional AZ.

First, we sought to address whether defects in the apposition of pre- and postsynaptic components are the result of degenerative processes. Distal NMJ regions are preferentially

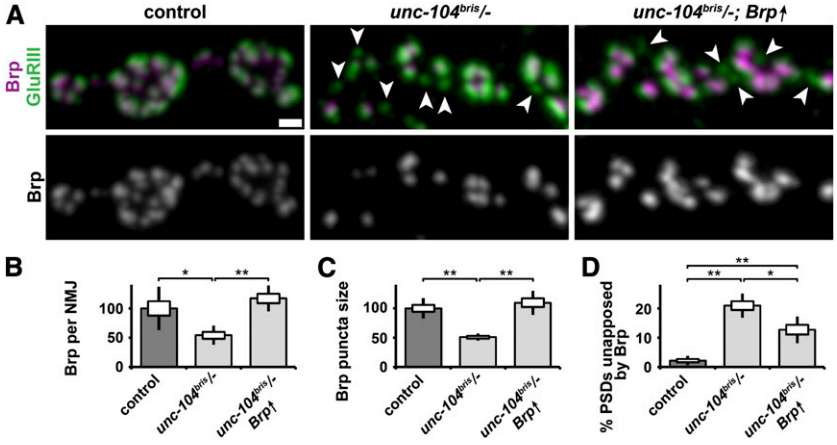

Figure 7 Brp overexpression does not rescue the AZ and PSD apposition defect in *unc-104^{bris}*/− larvae. (A) Confocal images of neuromuscular synapses immunostained with Brp (magenta and gray) and GluRIIC (green) in larvae of the following genotypes: *elav-Gal4/+;;* (control), *elav-Gal4/+;unc-104^{bris}/−* (*unc-104^{bris}/−*), and *elav-Gal4/+;unc-104^{bris}/−;UAS-Brp/+* (*unc-104^{bris}/−, Brp↑*). Arrows indicate PSDs unapposed by presynaptic Brp punctae. No Brp punctae without an apposed PSD were detected. Bar, 1 μm. Quantification of the abundance of Brp per NMJ (B), Brp quantity at a single puncta (C), and the percentage of PSDs unapposed by Brp (D). Experiments were performed at 29 °. The SEM is shown as a box, the SD as a black line. $*P < 0.05$, $**P < 0.01$.

affected by degenerative processes than proximal regions (Sherwood *et al.* 2004). In *unc-104^{bris}* larvae, however, unapposed PSDs were distributed in a "salt-and-pepper" pattern throughout the NMJ without obvious regional preference (Figure 5A, arrowheads), indicating that synaptic defects are likely caused by impaired synaptogenesis at the level of individual synapses.

Postsynaptic membranes at the *Drosophila* NMJ are a complex series of membrane folds (**sub**synaptic **r**eticulum, SSR) that develop only gradually upon presynaptic innervation and remain stable for hours after presynaptic retraction. Thus, terminal boutons positive for SSR marker but negative for the presynaptic membranes or synaptic vesicles (SV) are indicative of synapse retraction (Eaton *et al.* 2002). We visualized the presynaptic membrane, SSR, and SV with antibodies directed against HRP, the postsynaptic Discs-large protein (Dlg), and the vesicular glutamate transporter VGlut, respectively (Mahr and Aberle 2006). No signs of synapse retraction were observed in *unc-104^{bris}* larvae (Figure 5, B–E). Immunostaining analyses suggested delayed SSR development, as more synaptic boutons positive for HRP and VGlut but negative for Dlg (Figure 5, C and E; arrowheads) were observed in homozygous *unc-104^{bris}* larvae (WT: 0.15 ± 0.08, $n = 10$; *unc-104^{bris}*: 0.85 ± 0.08, $n = 10$; $P < 0.001$, Student's two-tailed *t*-test).

Second, the reliable apposition of PSDs and AZs might be disturbed by a rate-limited supply of Brp. The loss of Unc-104 function has been shown to affect cargo transport as quantified by cargo redistribution in the ventral nerve cord (Pack-Chung *et al.* 2007; Barkus *et al.* 2008). In control larvae, Unc-104 cargos are scant in the cortex and enriched in the neuropil. As previously reported for *unc-104* null embryos (Pack-Chung *et al.* 2007), this distribution is reversed in *unc-104^{bris}*/− larvae (Figure 6A). Furthermore, Brp density and the amount of Brp per NMJ in *unc-104^{bris}*/− larvae were reduced by 70 and 74%, respectively (Figure 6, B–D). Panneuronal expression of *unc-104^{mCherry}* was sufficient to rescue impairments in Brp transport (Figure 6, A–D).

As insufficient supply of Brp is a potential cause of the observed defects in the apposition of AZ and PSDs at *unc-104^{bris}* mutant synaptic terminals, we next rescued overall Brp abundance at NMJs (Figure 7, A and B) by panneuronal overexpression of Brp. Although Brp overexpression was sufficient to restore the overall abundance of Brp at the NMJ and the normal size of individual Brp punctae (Figure 7, A and C), the percentage of presynaptically unapposed PSDs was still four times higher in Brp-overexpressing *unc-104^{bris}*/− larvae compared to control larvae (Figure 7, A and D). Brp punctae are generally apposed by PSDs (Figure 7A), suggesting that the molecular mechanisms that prevent AZ formation in the perisynaptic regions of the NMJ are intact in *unc-104^{bris}*/− larvae. However, PSDs are not reliably apposed by Brp punctae (Figure 7A, arrowheads), indicating that Unc-104 might orchestrate the site-specific delivery of AZ components to defined synapses, thereby ensuring the proper allocation of Brp to all AZs.

Unc-104 is essential to restrict NMJ growth

Impairments in kinesin-1- and kinesin-3-based anterograde transport cause a reduction in NMJ size and a decrease in the number of synaptic boutons (Hurd and Saxton 1996; Barkus *et al.* 2008; Fuger *et al.* 2012). However, loss of the HSP-associated genes atlastin, spastin, and spichthyin induce NMJ overgrowth (Bayat *et al.* 2011).

To test whether impaired Unc-104 function leads to morphological changes at the synaptic terminal the following parameters were determined: NMJ length, NMJ size, PSDs per NMJ, boutons per NMJ, bouton size, and number of synapses per bouton. NMJ size is determined by the area of HRP staining. NMJ length is a measure of synaptic terminal outgrowth, while NMJ size and the number of PSDs per NMJ are a measure of both outgrowth and functional maturation. NMJs of *unc-104^{bris}*/− larvae were longer but not larger than NMJs in control larvae (Figure 8, A–C). The number of receptor fields per NMJ was decreased in *unc-104^{bris}*/− larvae (control: 277 ± 23, $n = 9$; *unc-104^{bris}*/−: 137 ± 8, $n = 9$; rescue: 226 ± 34, $n = 9$; control/*unc-104^{bris}*/−; $P < 0.001$, Kruskal–Wallis *H*-test). NMJs of mutant larvae consist of more but smaller synaptic boutons that contain fewer glutamate receptor fields than control boutons, suggesting that terminal outgrowth was not matched by proper functionalization (Figure 8, A and D–G).

The overgrowth of *unc-104^{bris}*/− NMJs was unexpected because previously described null and hypomorphic alleles

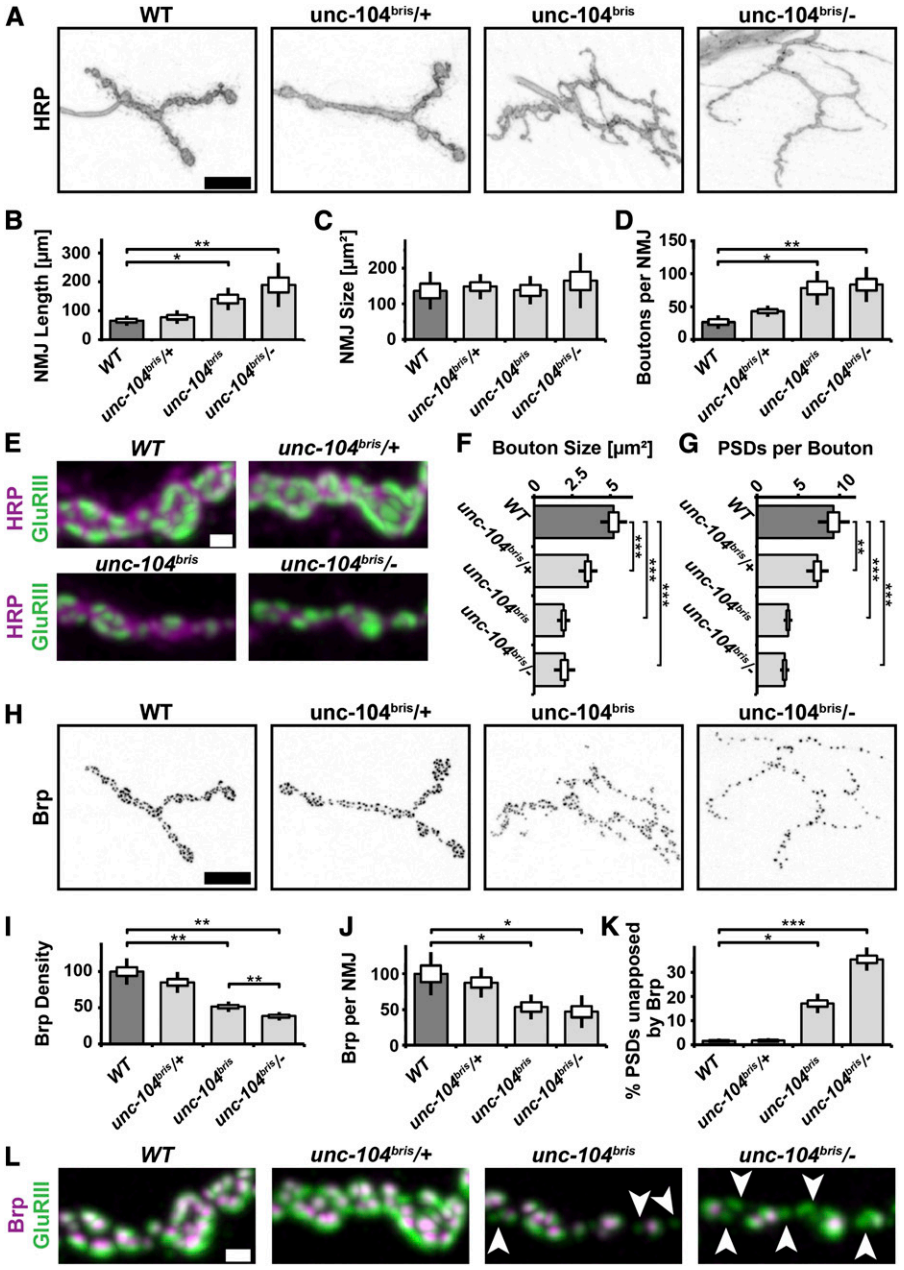

Figure 8 Altered NMJ morphology in *unc-104^{bris}*/− larvae. (A) NMJ 4, segment A2 of mid-third instar *Drosophila* wild-type, *unc-104^{bris}*/+, *unc-104^{bris}*, and *unc-104^{bris}*/− larvae were stained with antibodies against HRP (A and E), GluRIII (E and L), and Brp (L). Bars: A, 10 μm and E and L, 1 μm. NMJ length (B), NMJ size (C), bouton number (D), bouton size (F), and PSD per boutons (G) were determined. The same genotypes were stained with Brp (H). Brp density (I), Brp per NMJ (J), and percentage of PSDs unapposed by Brp (K) were quantified. The SEM is shown as a box, the SD as a black line. $*P < 0.05$, $**P < 0.01$, $***P < 0.001$. (L) PSDs unapposed by a presynaptic Brp puncta (arrowheads) were detected in *unc-104^{bris}* and *unc-104^{bris}*/− larvae.

cause defects in bouton formation and decreased number of boutons per NMJ, respectively (Pack-Chung *et al.* 2007; Barkus *et al.* 2008). We thus sought to (i) further investigate the nature of the putatively hypomorphic *unc-104^{bris}* mutation and (ii) verify that defects are solely caused by a presynaptic loss of Unc-104 function.

The phenotype of hypomorphic alleles is less severe when homozygous than transheterozygous to a null allele or a deletion. *unc-104^{bris}*/− larvae have stronger impairments in larval locomotion than homozygous *unc-104^{bris}* larvae. Generally, morphological defects were more pronounced in the former (Figure 8, A, B, D, E, and G–L); however, this difference was only statistically significant for Brp density (Figure 8I). Defects in bouton size do not follow this general trend (Figure 8F). Despite a smaller bouton size and less PSDs per bouton, no NMJ morphogenesis defects were observed in heterozygous *unc-104^{bris}*/+ larvae (Figure 8, E–G).

RNAi-mediated knockdown of Unc-104 in neurons (*elav-Gal4*, *D42-Gal4*) but not in muscles (*Mhc-Gal4*, *24B-Gal4*) is sufficient to induce lethality (data not shown). No Unc-104 signal was detectable in nonneuronal tissue (Pack-Chung *et al.* 2007). Panneuronal expression of *unc-104^{mCherry}* in the *unc-104* mutant background was sufficient to rescue defects in NMJ morphogenesis (Figure 9, A–G). Postsynaptic expression of *unc-104^{mCherry}* did not rescue neuromuscular morphological defects (Figure 10, A–C).

Overall, the morphological and behavioral analyses suggest that (i) *unc-104^{bris}* is a hypomorphic allele and (ii) defects are solely caused by loss of neuronal Unc-104 function.

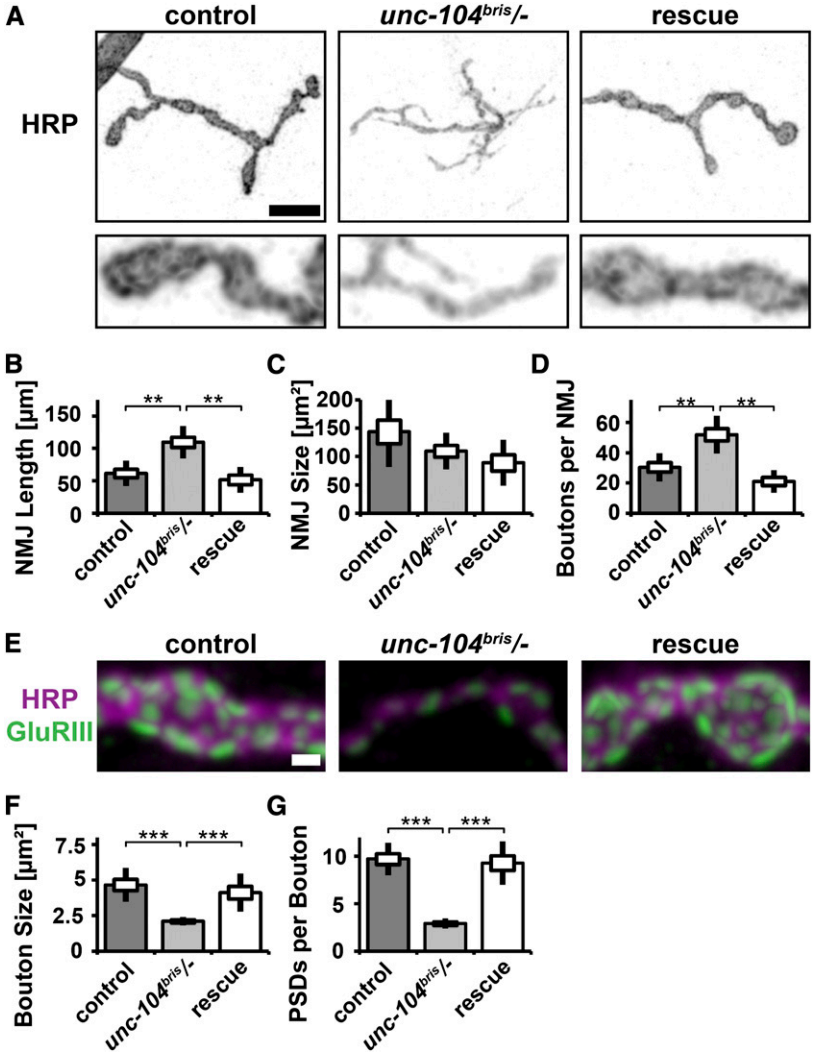

Figure 9 Panneuronal expression of *unc-104* rescues NMJ morphology defects in *unc-104*^{bris}/− larvae. (A) NMJ 4, segment A2 of mid-third instar *Drosophila* larvae of the following genotypes *elav-Gal4/+;;UAS-unc-104*^{mCherry}/+ (control), *unc-104*^{bris}/−;*UAS-unc-104*^{mCherry}/+ (*unc-104*^{bris}/−), and *elav-Gal4/+;unc-104*^{bris}/−;*UAS-unc-104*^{mCherry}/+ (rescue) were stained with antibodies against HRP (A and E) and GluRIII (E). Enlargements of A are shown in the lower panel. Bars: A, 10 µm and E, 1 µm. NMJ length (B), NMJ size (C), bouton number (D), bouton size (F), and PSDs per boutons (G) were determined. The SEM is shown as a box, the SD as a black line. $^{**}P < 0.01$, $^{***}P < 0.001$.

NMJ overgrowth is independent of presynaptic Brp abundance

NMJ overgrowth in *unc-104*^{bris} mutants, as quantified by NMJ length and the number of synaptic boutons, might be attributable to the loss of a specific function of Unc-104. Alternatively, defects in AZ assembly and maturation of synapses caused by the loss of Brp from some synapses might induce compensatory NMJ overgrowth.

We favor the former possibility for the following reasons: first, reduction in synaptic Brp levels alone, using transgenic RNAi, do not cause changes in overall NMJ size (Wagh *et al.* 2006). Second, Brp clusters calcium channels at AZs (Kittel *et al.* 2006). Reduced expression of the voltage-dependent calcium channel subunit cacophony (cac) or a point mutation (cac^{NT27}) that disrupts calcium entry and subsequent vesicle fusion limits NMJ growth rather than promoting NMJ overgrowth (Rieckhof *et al.* 2003).

If NMJ overgrowth is triggered as a compensatory response to the reduced level of synaptic Brp, further reduction or overexpression of Brp should exacerbate or rescue existing defects, respectively. To evaluate this hypothesis, we utilized previously validated *UAS-Brp* and *Brp-RNAi* constructs (Wagh *et al.* 2006). NMJ overgrowth was neither suppressed by the overexpression of Brp nor exacerbated by further reduction of Brp using RNAi (Figure 11, A–F). Defects in the enlargement and maturation of boutons persisted both after decreasing and increasing Brp abundance (Figure 11, E and F). We thus conclude that neither the overgrowth of NMJs nor the defects in bouton enlargement are secondary to reduced Brp abundance at the NMJ or its loss from a subset of AZs. Rather, they constitute novel functions of the Unc-104 FHA domain in limiting NMJ length and coordinating bouton enlargement.

Discussion

Dendrite morphogenesis

Sensory neurons that normally bear actin-rich filopodia display increased filopodial density in *unc-104*^{bris} mutants with no obvious defects in dendritic branching (observed herein and previously Medina *et al.* 2006). Interestingly, alterations in the structure of actin-rich dendritic spines were among the first neuroanatomical changes associated with mental retardation

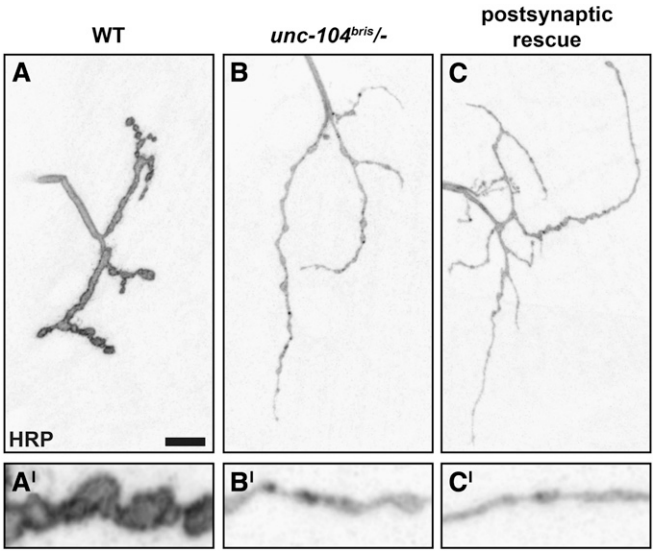

Figure 10 Postsynaptic expression of *unc-104* does not rescue morphological defects in *unc-104^{bris}*/− larvae. (A–C) NMJ 4, segment A2 of mid-third instar *Drosophila* larvae of the following genotypes: wild-type, *unc-104^{bris}*/−, and *unc-104^{bris}*/−*;24B-Gal4/UAS-unc-104^{mCherry}* (postsynaptic rescue) were stained for the membrane marker HRP. No rescue was detectable following postsynaptic expression of *unc-104^{mCherry}*. Enlargements are shown in the lower panel. Bar, 10 μm.

(Marin-Padilla 1972). More than 100 genes that coordinate dendrite arborization have been identified to date. Among these genes are two molecular motors: KIF5 (Hoogenraad *et al.* 2005) and dynein (Zhou *et al.* 2012). Our results suggest that Unc-104-based dendritic transport is important for maintaining correct dendrite morphology. Because no defects in dendrites were detected 16.5 h AEL, we concluded that impaired Unc-104 function during later outgrowth, branching, guidance, and pruning leads to the defects in larval dendrite morphology described here. Sensory neuron dendritic arbor morphology has been suggested to affect the ability of cells to perceive and transmit external stimuli (Hall and Treinin 2011). The resulting association between form and function might explain the divergence of dendritic morphologies. For example, class I, II, and III multidendritic sensory neurons, which respond to touch and serve as proprioceptors to coordinate larval contraction wave propagation, differ morphologically from class IV multidendritic neurons that sense noxious stimuli, such as heat, high-threshold mechanical stimuli, parasitoid wasps, and noxious light (Hall and Treinin 2011; Tsubouchi *et al.* 2012). *unc-104^{bris}* larvae are characterized by enhanced filopodia formation. As the number of dendritic sensory filopodia can correlate with the strength of the gentle touch response in class III multidendritic neurons (Tsubouchi *et al.* 2012), a detailed investigation of the behavioral responses to external stimuli in *unc-104^{bris}* larvae might enhance our understanding of the molecular pathways underlying sensory neuron dendrite structure and function.

Synapse apposition

unc-104^{bris} larvae are characterized by impairments in the reliable apposition of AZs and PSDs as quantified by staining for Brp (Wagh *et al.* 2006) and glutamate receptors. Brp clusters calcium channels at AZs and stabilizes T-bars, which are electron-dense presynaptic structures that have been shown to facilitate synaptic release (Kittel *et al.* 2006). In wild-type larvae, primarily very young (<3 h), immature synapses are Brp negative (Rasse *et al.* 2005). Because Brp-negative synapses have a low vesicle release probability, the accumulation of Brp at nascent AZs is an important step during synapse maturation (Rasse *et al.* 2005; Kittel *et al.* 2006; Schmid *et al.* 2008). The high percentage of Brp-negative synapses in the *unc-104^{bris}* mutant suggests that synapse maturation is impaired either by rate-limiting axonal transport of Brp, defective delivery of Brp to AZs, or the inability to stabilize synaptic Brp. Restoration of Brp abundance at NMJs in *unc-104^{bris}* larvae ameliorates but does not rescue defects in the apposition of AZs and PSDs. We thus propose that the R561H mutation in Unc-104's FHA domain might disrupt a previously unknown function of Unc-104 in orchestrating the site-specific delivery of Brp to defined synapses.

The specificity of defects caused by the R561H mutation is further supported by the analysis of *unc-104^{170}*/− mutant embryos. The total amount of Brp per NMJ at 21 h AEL was more severely reduced than in *unc-104^{bris}* larvae (Pack-Chung *et al.* 2007). Nonetheless, no defects in the apposition of AZ and PSDs were reported; most PSDs were apposed by a weak Brp-positive signal (Pack-Chung *et al.* 2007).

The precise coordination of synaptic cargo delivery to defined synapses is important to functionalize and facilitate these synapses (for review see Vitureira *et al.* 2011; Clarke *et al.* 2012). Intact Unc-104/KIF1A-based cargo trafficking might, reminiscent of kinesin-1-based long-range transport (Puthanveettil *et al.* 2008), be important for the late phase of long-term potentiation (Bliss and Lomo 1973), which is highly relevant in the context of learning and memory. Indeed, environmental enrichment has been shown to be sufficient to induce brain-derived neurotrophic factor (BDNF)-dependent up-regulation of KIF1A (Kondo *et al.* 2012). The resulting hippocampal synaptogenesis and learning enhancement is absent in transheterozygous *Bdnf$^{+/-}$* and *Kif1a$^{+/-}$* mutant mice, highlighting that Unc-104/KIF1A is essential for experience-dependent neuroplasticity (Kondo *et al.* 2012).

We propose that the presynaptic mechanism underlying neuroplasticity depends on both Unc-104-based long-range axonal transport and the site-specific delivery of synaptic cargo to defined synapses. Both processes might be perturbed by mutation of the R561 residue that localizes to the β11-loop of the FHA domain. The corresponding residue (R583) in KIF1A has been suggested to further stabilize kinesin-3 dimers by electrostatic interaction with the E499 residue (Huo *et al.* 2012). Further investigation of the effects of R561H on the activation and deactivation of Unc-104 upon cargo loading and release might provide novel insights into the biomechanics of kinesin-3-based cargo trafficking.

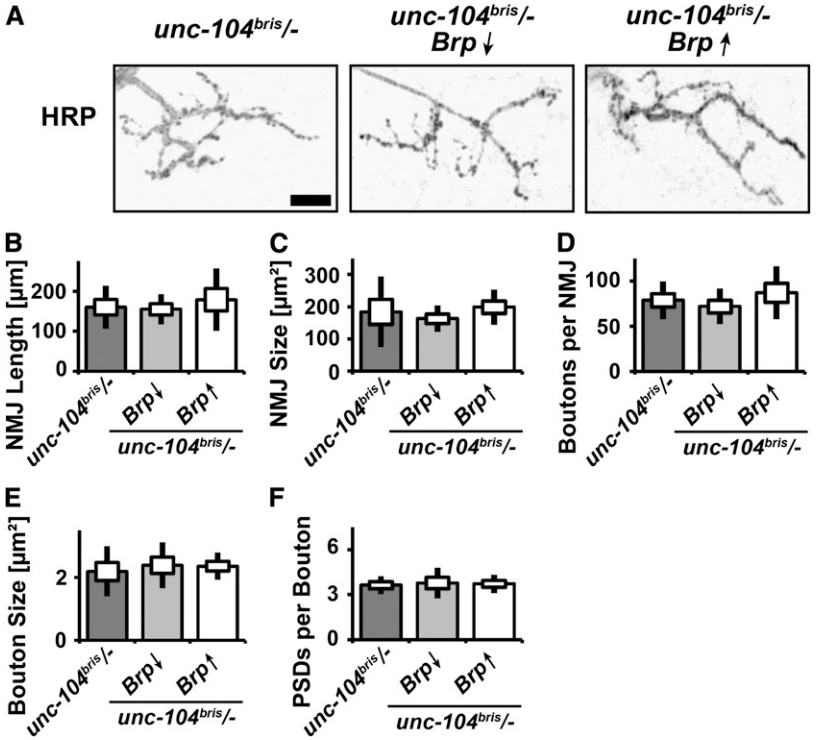

Figure 11 Altering Brp abundance does not overtly alter NMJ morphology. (A–F) NMJ 4, segment A2 of mid-third instar *Drosophila* larvae of the following genotypes: *elav-Gal4/+;unc-104^{bris}/−* (*unc-104^{bris}/−*), *elav-Gal4/+;unc-104^{bris}/−,UAS-Brp-RNAi/+* (Brp↓), and *elav-Gal4/+; unc-104^{bris}/−;UAS-Brp/+* (Brp↑) were stained for the membrane marker HRP (A). The following characteristics of NMJs were determined: NMJ length (B), NMJ size (C), bouton number (D), bouton size (E), and PSDs per bouton (F). Bar, 10 µm. The SEM is shown as a box, the SD as a black line.

Molecular pathways underlying structural defects at NMJs

The herein described overgrowth of NMJs in *unc-104^{bris}* larvae was surprising as both impairments in kinesin-1- and kinesin-3-based anterograde transport were reported to result in reductions in both NMJ size and synaptic bouton number (Hurd and Saxton 1996; Barkus *et al.* 2008; Fuger *et al.* 2012). Conversely, phenotypic comparison with other HSP-associated genes revealed that the NMJ overgrowth is a common phenotype in HSP fly models. Null alleles in atlastin, spastin, and spichthyin result in synaptic bouton number increases of 17, 60, and 100% respectively (Bayat *et al.* 2011).

Interestingly, in *unc-104^{bris}/−* larvae, NMJ overgrowth and defects in bouton enlargement and maturation seem to be independent of Unc-104's role in fast axonal transport of AZ components and might thus represent novel functions of Unc-104.

Defects in bidirectional communication between muscles and motoneurons might induce NMJ overgrowth. The absence of bone morphogenetic protein (BMP)-signaling suppressors, such as daughters against decapentaplegic and the HSP-related gene spichthyin, causes NMJ overgrowth (Sweeney and Davis 2002; Wang *et al.* 2007). Thus, the NMJ overgrowth observed in *unc-104^{bris}* larvae is consistent with potential overactivation of BMP signaling. Due to the importance of BMP signaling in synapse stabilization (Eaton and Davis 2005), its overactivation might prevent the elimination of functionally impaired synaptic terminals in *unc-104^{bris}* mutant larvae.

Conclusions

Our identification of a novel *unc-104* allele highlights the importance of kinesin activity during later stages of neuronal development. The results described here shed light on three previously unknown roles of Unc-104. First, it is important for maintaining correct dendritic morphology. Second, Unc-104 is required for the reliable apposition of AZs and glutamate receptor fields. Third, Unc-104 is important to limit NMJ outgrowth as measured by NMJ length and bouton number.

Alterations in dendritic and synaptic terminal maturation are independently associated with mental retardation and neurodegeneration. The fact that a single amino acid substitution of arginine for histidine in the FHA domain of Unc-104 is sufficient to perturb all these processes presents an ideal tool to decipher the biophysical underpinnings of neurodevelopmental disorders.

Further study is needed to decipher the exact role of Unc-104 in orchestrating synaptic terminal outgrowth and functional maturation. Studies of the FHA domain in a biochemical setting may provide novel insights into (i) the biomechanics of kinesin-3-based cargo trafficking, (ii) Unc-104's roles in synapse development and synaptic plasticity, and (iii) the molecular mechanism underlying HSP and neurodevelopmental diseases in which synapses might fail to mature.

Acknowledgments

We thank Christian Hünefeld, Roman Beck, Jörg Odenthal, Raphael S. Zinser, Shabab Hannan, Junyi Zhu, and Jutta Bloschies for help and/or advice. We thank Stephan Sigrist, Hermann Aberle, Ann Goldstein, and Thomas Schwarz for providing reagents. This work was supported by grants from the Deutsche Forschungsgemeinschaft (RA 1804/2-1 to T.M.R.) and National Institute of Neurological Disorders and

Stroke (NS080108 to J.E.B.). Y.V.Z. was supported by a fellowship of the China Scholarship Council.

Literature Cited

Barkus, R. V., O. Klyachko, D. Horiuchi, B. J. Dickson, and W. M. Saxton, 2008 Identification of an axonal kinesin-3 motor for fast anterograde vesicle transport that facilitates retrograde transport of neuropeptides. Mol. Biol. Cell 19: 274–283.

Bayat, V., M. Jaiswal, and H. J. Bellen, 2011 The BMP signaling pathway at the Drosophila neuromuscular junction and its links to neurodegenerative diseases. Curr. Opin. Neurobiol. 21: 182–188.

Bliss, T. V., and T. Lomo, 1973 Long-lasting potentiation of synaptic transmission in the dentate area of the anaesthetized rabbit following stimulation of the perforant path. J. Physiol. 232: 331–356.

Cai, Q., P. Y. Pan, and Z. H. Sheng, 2007 Syntabulin-kinesin-1 family member 5B-mediated axonal transport contributes to activity-dependent presynaptic assembly. J. Neurosci. 27: 7284–7296.

Clarke, G. L., J. Chen, and H. Nishimune, 2012 Presynaptic Active Zone Density during Development and Synaptic Plasticity. Front Mol Neurosci 5: 12.

Corty, M. M., B. J. Matthews, and W. B. Grueber, 2009 Molecules and mechanisms of dendrite development in Drosophila. Development 136: 1049–1061.

Dietzl, G., D. Chen, F. Schnorrer, K. C. Su, Y. Barinova *et al.*, 2007 A genome-wide transgenic RNAi library for conditional gene inactivation in Drosophila. Nature 448: 151–156.

Eaton, B. A., and G. W. Davis, 2005 LIM Kinase1 controls synaptic stability downstream of the type II BMP receptor. Neuron 47: 695–708.

Eaton, B. A., R. D. Fetter, and G. W. Davis, 2002 Dynactin is necessary for synapse stabilization. Neuron 34: 729–741.

Erlich, Y., S. Edvardson, E. Hodges, S. Zenvirt, P. Thekkat *et al.*, 2011 Exome sequencing and disease-network analysis of a single family implicate a mutation in KIF1A in hereditary spastic paraparesis. Genome Res. 21: 658–664.

Fuger, P., L. B. Behrends, S. Mertel, S. J. Sigrist, and T. M. Rasse, 2007 Live imaging of synapse development and measuring protein dynamics using two-color fluorescence recovery after photo-bleaching at Drosophila synapses. Nat. Protoc. 2: 3285–3298.

Fuger, P., V. Sreekumar, R. Schule, J. V. Kern, D. T. Stanchev *et al.*, 2012 Spastic paraplegia mutation N256S in the neuronal microtubule motor KIF5A disrupts axonal transport in a Drosophila HSP model. PLoS Genet. 8: e1003066.

Gao, F. B., J. E. Brenman, L. Y. Jan, and Y. N. Jan, 1999 Genes regulating dendritic outgrowth, branching, and routing in Drosophila. Genes Dev. 13: 2549–2561.

Hall, D. H., and E. M. Hedgecock, 1991 Kinesin-related gene unc-104 is required for axonal transport of synaptic vesicles in C. elegans. Cell 65: 837–847.

Hall, D. H., and M. Treinin, 2011 How does morphology relate to function in sensory arbors? Trends Neurosci. 34: 443–451.

Hirokawa, N., and Y. Noda, 2008 Intracellular transport and kinesin superfamily proteins, KIFs: structure, function, and dynamics. Physiol. Rev. 88: 1089–1118.

Hirokawa, N., S. Niwa, and Y. Tanaka, 2010 Molecular motors in neurons: transport mechanisms and roles in brain function, development, and disease. Neuron 68: 610–638.

Hoogenraad, C. C., A. D. Milstein, I. M. Ethell, M. Henkemeyer, and M. Sheng, 2005 GRIP1 controls dendrite morphogenesis by regulating EphB receptor trafficking. Nat. Neurosci. 8: 906–915.

Huo, L., Y. Yue, J. Ren, J. Yu, J. Liu *et al.*, 2012 The CC1-FHA tandem as a central hub for controlling the dimerization and activation of kinesin-3 KIF1A. Structure 20: 1550–1561.

Hurd, D. D., and W. M. Saxton, 1996 Kinesin Mutations Cause Motor Neuron Disease Phenotypes by Disrupting Fast Axonal Transport in Drosophila. Genetics 144: 1075–1085.

Kittel, R. J., C. Wichmann, T. M. Rasse, W. Fouquet, M. Schmidt *et al.*, 2006 Bruchpilot promotes active zone assembly, $Ca2^+$ channel clustering, and vesicle release. Science 312: 1051–1054.

Klebe, S., A. Lossos, H. Azzedine, E. Mundwiller, R. Sheffer *et al.*, 2012 KIF1A missense mutations in SPG30, an autosomal recessive spastic paraplegia: distinct phenotypes according to the nature of the mutations. Eur. J. Hum. Genet. 20: 645–649.

Kondo, M., Y. Takei, and N. Hirokawa, 2012 Motor protein KIF1A is essential for hippocampal synaptogenesis and learning enhancement in an enriched environment. Neuron 73: 743–757.

Mahr, A., and H. Aberle, 2006 The expression pattern of the Drosophila vesicular glutamate transporter: a marker protein for motoneurons and glutamatergic centers in the brain. Gene Expr. Patterns 6: 299–309.

Marin-Padilla, M., 1972 Structural abnormalities of the cerebral cortex in human chromosomal aberrations: a Golgi study. Brain Res. 44: 625–629.

Marrus, S. B., S. L. Portman, M. J. Allen, K. G. Moffat, and A. DiAntonio, 2004 Differential localization of glutamate receptor subunits at the Drosophila neuromuscular junction. J. Neurosci. 24: 1406–1415.

Medina, P. M., L. L. Swick, R. Andersen, Z. Blalock, and J. E. Brenman, 2006 A novel forward genetic screen to identify mutations affecting larval neuronal dendrite development in Drosophila melanogaster. Genetics 172: 2325–2335.

Nangaku, M., R. Sato-Yoshitake, Y. Okada, Y. Noda, R. Takemura *et al.*, 1994 KIF1B, a novel microtubule plus end-directed monomeric motor protein for transport of mitochondria. Cell 79: 1209–1220.

O'Farrell, F., S. S. Esfahani, Y. Engstrom, and P. Kylsten, 2008 Regulation of the Drosophila lin-41 homologue dappled by let-7 reveals conservation of a regulatory mechanism within the LIN-41 subclade. Dev. Dyn. 237: 196–208.

Ohashi, S., K. Koike, A. Omori, S. Ichinose, S. Ohara *et al.*, 2002 Identification of mRNA/protein (mRNP) complexes containing Puralpha, mStaufen, fragile X protein, and myosin Va and their association with rough endoplasmic reticulum equipped with a kinesin motor. J. Biol. Chem. 277: 37804–37810.

Pack-Chung, E., P. T. Kurshan, D. K. Dickman, and T. L. Schwarz, 2007 A Drosophila kinesin required for synaptic bouton formation and synaptic vesicle transport. Nat. Neurosci. 10: 980–989.

Parks, A. L., K. R. Cook, M. Belvin, N. A. Dompe, R. Fawcett *et al.*, 2004 Systematic generation of high-resolution deletion coverage of the Drosophila melanogaster genome. Nat. Genet. 36: 288–292.

Puthanveettil, S. V., F. J. Monje, M. C. Miniaci, Y. B. Choi, K. A. Karl *et al.*, 2008 A new component in synaptic plasticity: upregulation of kinesin in the neurons of the gill-withdrawal reflex. Cell 135: 960–973.

Qin, G., T. Schwarz, R. J. Kittel, A. Schmid, T. M. Rasse *et al.*, 2005 Four different subunits are essential for expressing the synaptic glutamate receptor at neuromuscular junctions of Drosophila. J. Neurosci. 25: 3209–3218.

Rasse, T. M., W. Fouquet, A. Schmid, R. J. Kittel, S. Mertel *et al.*, 2005 Glutamate receptor dynamics organizing synapse formation in vivo. Nat. Neurosci. 8: 898–905.

Rieckhof, G. E., M. Yoshihara, Z. Guan, and J. T. Littleton, 2003 Presynaptic N-type calcium channels regulate synaptic growth. J. Biol. Chem. 278: 41099–41108.

Riviere, J. B., S. Ramalingam, V. Lavastre, M. Shekarabi, S. Holbert *et al.*, 2011 KIF1A, an axonal transporter of synaptic vesicles, is mutated in hereditary sensory and autonomic neuropathy type 2. Am. J. Hum. Genet. 89: 219–230.

Ryder, E., M. Ashburner, R. Bautista-Llacer, J. Drummond, J. Webster *et al.*, 2007 The DrosDel deletion collection: a Drosophila genome-wide chromosomal deficiency resource. Genetics 177: 615–629.

Schmid, A., S. Hallermann, R. J. Kittel, O. Khorramshahi, A. M. Frolich *et al.*, 2008 Activity-dependent site-specific changes of glutamate receptor composition in vivo. Nat. Neurosci. 11: 659–666.

Sherwood, N. T., Q. Sun, M. Xue, B. Zhang, and K. Zinn, 2004 Drosophila spastin regulates synaptic microtubule networks and is required for normal motor function. PLoS Biol. 2: e429.

Sweeney, S. T., and G. W. Davis, 2002 Unrestricted synaptic growth in spinster-a late endosomal protein implicated in TGF-beta-mediated synaptic growth regulation. Neuron 36: 403–416.

Thibault, S. T., M. A. Singer, W. Y. Miyazaki, B. Milash, N. A. Dompe *et al.*, 2004 A complementary transposon tool kit for Drosophila melanogaster using P and piggyBac. Nat. Genet. 36: 283–287.

Tsubouchi, A., J. C. Caldwell, and W. D. Tracey, 2012 Dendritic filopodia, Ripped Pocket, NOMPC, and NMDARs contribute to the sense of touch in Drosophila larvae. Curr. Biol. 22: 2124–2134.

van den Berg, R., and C. C. Hoogenraad, 2012 Molecular motors in cargo trafficking and synapse assembly. Adv. Exp. Med. Biol. 970: 173–196.

Verhey, K. J., and J. W. Hammond, 2009 Traffic control: regulation of kinesin motors. Nat. Rev. Mol. Cell Biol. 10: 765–777.

Verhey, K. J., N. Kaul, and V. Soppina, 2011 Kinesin assembly and movement in cells. Annu Rev Biophys 40: 267–288.

Vitureira, N., M. Letellier, and Y. Goda, 2011 Homeostatic synaptic plasticity: from single synapses to neural circuits. Curr. Opin. Neurobiol. 22: 516–521.

Wagh, D. A., T. M. Rasse, E. Asan, A. Hofbauer, I. Schwenkert *et al.*, 2006 Bruchpilot, a protein with homology to ELKS/CAST, is required for structural integrity and function of synaptic active zones in Drosophila. Neuron 49: 833–844.

Wang, X., W. R. Shaw, H. T. Tsang, E. Reid, and C. J. O'Kane, 2007 Drosophila spichthyin inhibits BMP signaling and regulates synaptic growth and axonal microtubules. Nat. Neurosci. 10: 177–185.

Zhai, R. G., P. R. Hiesinger, T. W. Koh, P. Verstreken, K. L. Schulze *et al.*, 2003 Mapping Drosophila mutations with molecularly defined P element insertions. Proc. Natl. Acad. Sci. USA 100: 10860–10865.

Zhang, Y., P. Fuger, S. B. Hannan, J. V. Kern, B. Lasky *et al.*, 2010 In vivo imaging of intact Drosophila larvae at sub-cellular resolution. J. Vis. Exp. 10: pii: 2249.

Zhou, B., Q. Cai, Y. Xie, and Z. H. Sheng, 2012 Snapin Recruits Dynein to BDNF-TrkB Signaling Endosomes for Retrograde Axonal Transport and Is Essential for Dendrite Growth of Cortical Neurons. Cell Rep 2: 42–51.

Communicating editor: P. K. Geyer

GENETICS

Supporting Information
http://www.genetics.org/lookup/suppl/doi:10.1534/genetics.113.151639/-/DC1

The Kinesin-3, Unc-104 Regulates Dendrite Morphogenesis and Synaptic Development in *Drosophila*

Jeannine V. Kern, Yao V. Zhang, Stella Kramer, Jay E. Brenman, and Tobias M. Rasse

DOI: 10.1534/genetics.113.151639

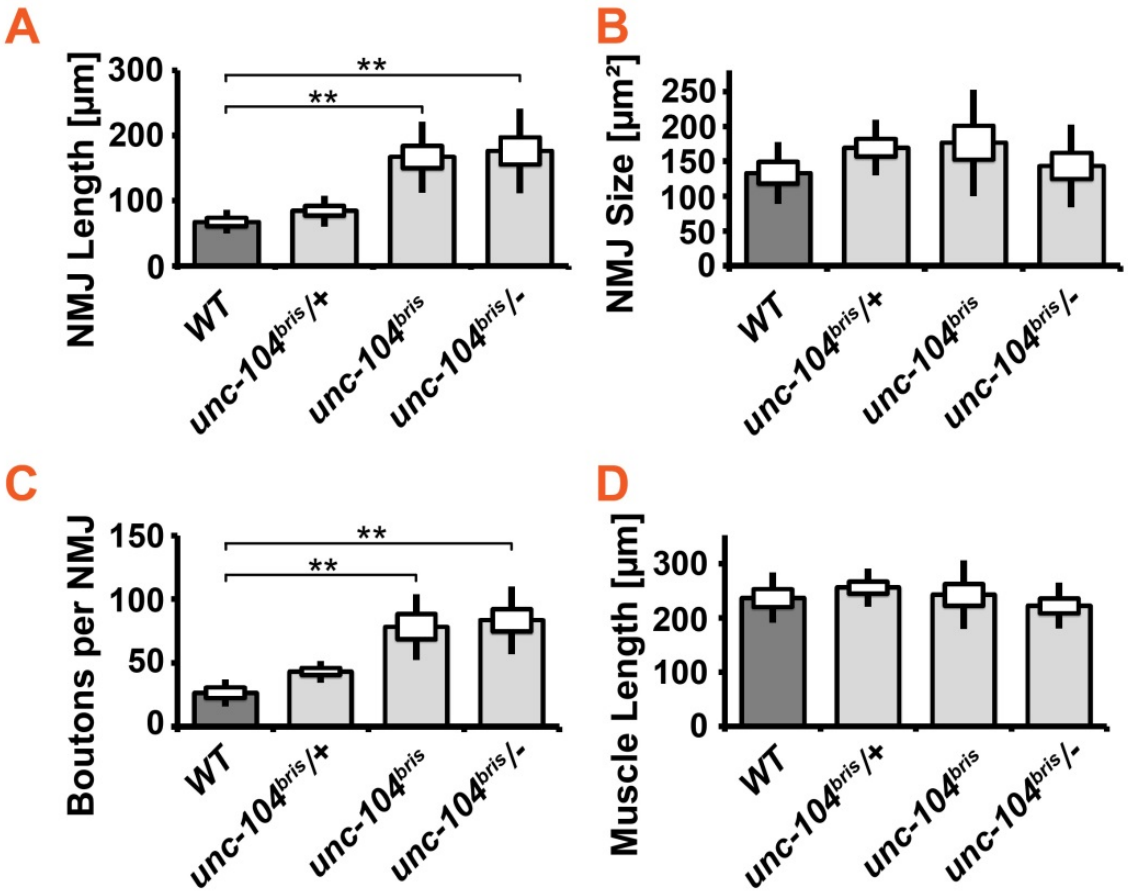

Figure S1 Altered NMJ morphology in unc-104^{bris}/- larvae. Analysis of NMJ 4, Segment A2 of mid third instar Drosophila wild-type, unc-104^{bris}/+, unc-104^{bris}, and unc-104^{bris}/- larvae. Non-normalized raw data of NMJ length **(A)**, NMJ size **(B)**, bouton number **(C)** is shown. Data normalized by (D) the muscle length or area is shown in Figure 8 B,C,D. The SEM is shown as a box, the SD as a black line. ** p<0.01.

File S1

Sequence raw data for genes listed in Figure 2B

unc-104^{bris} R561H

CGCTGCTCAGAAACGATGGTGTGGAGCATGCGCGGGATTCTCACCGAAGAAGACTCCGCATTTGGTCAACCTAAACGAGGATCCCAATC
TGTCTGAGTGTCTGCTTTACTACATCAAGGAGGGTCTAACTCGGTTGGGTACCCATGAAGCAAATGTGCCCCAGGACATTCAGCTCTCCG
GATCGCACATCCTCAAGGAGCACTGCACCTTTGAGAACAAGAACAGCACGGTTACATTGCTGCCACACAAGGATGCTATCATCTATGTAA
ATGGACGCAAGTTGGTTGAACCGGAGGTTCTTAAGACCGGTTCTCACGTGATCCTCGGAAAGAACCACGTGTTCCGCTTTACCAATCCAG
AACAGGCACGCGAATTACGGGATAAGATCGAGACCGAAAATGAGGCTGAGAACGAAGTGGAGAAGACAGACACCCAGCAGGTGGACT
GGAACTTTGCCCAGTGCGAATTGCTCGAGAAGCAAGGCATTGATCTAAAAGCTGAAATGAAGAAGCGTTTAGACAACTTGGAGGAACA
GTACAAGCGGGAGAAACTTCAGGCCGATCAGCAATTCGAGGAGCAGCGCAAAACGTACGAGGCTCGCATCGATGCTTTGCAAAAACAG
GTTAGAAGACAAATCCAATGAA

unc-104^{bris} V772L

AAGGAGCCAGTGCCGTTTCCGTTGAGTTAAAGAAGAAGGTACATAGTTTACGCCTATTACTTAACATAATAGATTAGAGATCATATACTT
AAATATTTATTTCAGGTACAATTCCAATTTACTCTCTTGACCGACACCTTGTACTCTCCTTTGCCGCCTGAGCTGGCATCCACTGTGGCTCCT
TTGCATCAGGAGGATGAGTTCGGAGCTCCACCTGTCTCTAAGACCTTGGTGGCCGTCGAAGTTACCGATACTAAGAACGGAGCCACTCA
CCACTGGTCTCTGGAGAAGTTACGGTAGGTTCTTTTATATCCGGAAATCCATGCGAATTCCTGCTACTCCCTCACATTCATTCTTCTCTGCA
CTTTGGTTAAAATTAAAAAAAAAAAGCTGGCTTTTGATTTGAGTTGAATATTATTTAAATAATACGTGCATGGGGGTTGTAGTTCATGGATT
CTAGTTTCTATCAAACGCTCTAAAATTTGTTGGTTACTTTTATAACTTTGGCTGTAAAAAGCAGAAAAAATCACAA

unc-104^{bris} D1073E

TTCAAGATTTCAACCAAACCAAAACATCGTGCTTAGCCAAAACCGTAGACGTGGGTGCACATGGTAGTGGTCCAAATTTGGGACTACGCA
CTGGCTGACTGATTGGTATGCTCGGTGGCAACATGCGACGTGGTGGTGGCCGGGAAACAAACTCCTGTTTGGCATCCTTATGCAATGGG
TGCGTCTGGTAGTGCCCAAATATCTTGAACATTATGGGTTGGGTCTTCAAATACTCGATGAAGGATTTGGTTACGGGTACAGTTATCTAC
AGAAAAGATAACAGTTAATAATTGATATGGTGGAAAGCTCTTGGTAATCTTGTAATCTTCCACTTACGTTCTGAACATGGTAGAAGCCTA
GAGGAGCACCCGATGCCGAATTCTTGACGGGTTCGGTGGAGAAAGCCTCCTCATGACGATGCAAAAAGCTGTAAAGGTAACAGTTTATA
AACCACAAACCTAAAGTTAATTTCCGAAAGATTACGTACTTGAACTGGCAGAAGATATCGGCATATTCAGCCCCAATACCAGTGGCCTGT
AGCACAGTGACCCGGAAAGTGAACTCCTTGCCCACCTGCAGATGCTCGCCAGGCTCCTCCGAATTTTCGTGGCACTCGGATGCGGAGTTA
GAGTCAATGCCACGACCAGAG

unc-104^{bris} V1170M

ACGTCGTCGAGTCCAGGCAGCCTCAAACGGTAGAAAGATCTATCATCTCCGGGCACCTCCAAAGCCTCGCCTGGGAACAAGCCCAAAGA
TAAGACACAGGCGTCTTCGTCCTGTTCGTCGGATGACTCCGGTGTATTGCGGATACGTCCAACCACCAACTCATTGATGTCCTTCCACTTC
ATCTCGGTTGTGGGCTCATGTACGATAGTAATACGAATGCGCCGCTGGATGCCCTGATGCAAGAGGAACAGTCCGCGGCAGGGAAGAT
CATCGCTGTGCTCCACCACCTGTTGACAAATTTATGTTTGGATTATTGCGTGTGAGACTGGGAAAGATTACATCTGCGCCATACTAACCGA
TGGCACATATTCTCCATTGGGAGCCAATTCACAGATTTCAAACCAAACCAAAACATCGTGCTTAGCCAAAACCGTAGACGTGGGTGCACA
TGGTAGTGGTCCAAATTTGGGACTACGCACTGGCTGACTGATTGGTATGCTCGGTGGCAACATGCGACGTGGTGGTGGCCGGGAAACA
AACTCCTGTTTGGCATCCTTATGCAATGGGTGCGTCTGGTAGTGCCCAAAATATCTTGGA

unc-104^{bris} A1405V

TTGTGACACCAGCTCTACTTATGTGCGCGGCGAGGAGAATCTTCATGGCTGGAGGCCAAGGGGTGACTCCCTGATCTTCGATCACCAGT
GGGAGCTGGAGAAACTCACCAGACTTGAAGAGGTTGGACGCATGCGGCACTTGCTTCTGCTGCGCGAACGTCTGGGCATGGACACCAA
CCCGAATCCGACCACCAAGACCGAGAAGGATGTTTGCAATCTAGCTGCTCGGGCAGTCACATCACCCGTACATATGGTCATTCCACAATC
GCCGCAGACTCCGGTCAAGGACCCACAGCAAATCATTCCAGAACGCGAGTACAACCAACGGGAGCAGGATCTCATGCTTAAATGCTTAA
AATTGGTGCAGGGTGAGTTAATACTGAGACTTACCAAGCGTTCCATTCACTCTATTCTAAATTCATTTAAGGACGCTATACTAAGAGCGA
GGCCAACGATACGCAAACTCAGTCGGATGTTTCGCCTAGCGATGAGGGATGTGCCGATATGACCGTCAGCTGCATCTCCAGCAATTCCAT
GGAGTGAGTAGTCGTTTAGCCACCCGTATAAACACACCACCCACACCAGCACCACCCATCTTAGTTAGCTG

parental R561R

CGGCTGCGCACGTATGATGGATATCAGTTGGCGTATTCTCACCGAAGAAGACTCCGCATTTGGTCAACCTAAACGAGGATCCCAATCTGT
CTGAGTGTCTGCTTTACTACATCAAGGAGGGTCTAACTCGGTTGGGTACCCATGAAGCAAATGTGCCCCAGGACATTCAGCTCTCCGGAT
CGCACATCCTCAAGGAGCACTGCACCTTTGAGAACAAGAACAGCACGGTTACATTGCTGCCACACAAGGATGCTATCATCTATGTAAATG
GACGCAAGTTGGTTGAACCGGAGGTTCTTAAGACCGGTTCTCGCGTGATCCTCGGAAAGAACCACGTGTTCCGCTTTACCAATCCAGAAC
AGGCACGCGAATTACGGGATAAGATCGAGACCGAAAATGAGGCTGAGAACGAAGTGGAGAAGACAGACACCCAGCAGGTGGACTGGA
ACTTTGCCCAGTGCGAATTGCTCGAGAAGCAAGGCATTGATCTAAAAGCTGAAATGAAGAAGCGTTTAGACAACTTGGAGGAACAGTAC
AAGCGGGAGAAACTTCAGGCCGATCAGCAATTCGAGGAGCAGCGCAAAACGTACGAGGCTCGCATCGATGCTTTGCAAACGGGAGGAA
ACCCCCCCCCCCCCCCTGCAGAGGGCACCCCAGAAAACTTAAGAAAAGGAATTTTCTCCCTGAAAAAAACACCCCATTTTAACGATATCTT
TAAGGGGGGGCCCGTGGGTCATCATCTT

parental V772L

AGGAGCCAGTGCCGTTTCCGTTGAGTTAAGAAGAAGGTACATAGTTTACGCCTATTACTTAACATAATAGATTAGAGATCATATACTTAA
ATATTTATTTCAGGTACAATTCCAATTTACTCTCTTGACCGACACCTTGTACTCTCCTTTGCCGCCTGAGCTGGCATCCACTGTGGCTCCTTT
GCATCAGGAGGATGAGTTCGGAGCTCCACCTGTCTCTAAGACCTTGGTGGCCGTCGAAGTTACCGATACTAAGAACGGAGCCACTCACC
ACTGGTCTCTGGAGAAGTTACGGTAGGTTCTTTTATATCCGGAAATCCATGCGAATTCCTGCTACTCCCTCACATTCATTCTTCTCTGCACT
TTGGTTAAAATTAAAAAAAATAGCAGGCTTTTGATTTGAGTTGAATATTATTTAAATAATCCGTGCATGATGGTTGTAAATAATGGATTCC
AATGTCCCTCAAACGCTCTCTCATTTGATGGGTACTTGTATAACTTTGGGTGTAAACATGGGCCCACATAAA

parental D1073E

AATCCAGATTTCAACCAACCAAAACATCGTGCTTAGCCAAAACCGTAGACGTGGGTGCACATGGTAGTGGTCCAAATTTGGGACTACGCA
CTGGCTGACTGATTGGTATGCTCGGTGGCAACATGCGACGTGGTGGTGGCCGGGAAACAAACTCCTGTTTGGCATCCTTATGCAATGGG
TGCGTCTGGTAGTGCCCAAATATCTTGAACATTATGGGTTGGGTCTTCAAATACTCGATGAAGGATTTGGTTACGGGTACAGTTATCTAC
AGAAAAGATAACAGTTAATAATTGATATGGTGGAAAGCTCTTGGTAATCTTGTAATCTTCCACTTACGTTCTGAACATGGTAGAAGCCTA
GAGGAGCACCCGATGCCGAATTCTTGACGGGTTCGGTGGAGAAAGCCTCCTCATGACGATGCAAAAAGCTGTAAAGGTAACAGTTTATA
AACCACAAACCTAAAGTTAATTTCCGAAAGATTACGTACTTGAACTGGCAGAAGATATCGGCATATTCAGCCCCAATACCAGTGGCCTGT
AGCACAGTGACCCGGAAAGTGAACTCCTTGCCCACCTGCAGATGCTCGCCAGGCTCCTCCGAATTTTCGTGGCACTCGGATGCGGAGTTA
GAGTCAATGCCACGACCAGAGTCCACATCCTCAAGTTCTTTTACAAATAATGAATATGAAA

parental V1170M

GTTCTCTGCACATCTCGCTGCTGCTCGATTTTTTGTTCCCGGCCACCACCACGTCGCATGCACATAAAGGCTTCCCTGGTCGAGACGTTCAT
CCATTGCCACCGGGCATACCAATCAGTCAGCCAGTGCGTAGTCCCAAATTTGGACCACTACCATGTGCACCCACGTCTACGGTTTTGGCTA
AGCACGATGTTTTGGTTTGGTTTGAAATCTGTGAATTGGCTCCCAATGGAGAATATGTGCCATCGGTTAGTATGGCGCAGATGTAATCTT
TCCCAGTCTCACACGCAATAATCCAAACATAAATTTGTCAACAGGTGGTGGAGCACAGCGATGATCTTCCCTGCCGCGGACTGTTCCTCTT
GCATCAGGGCATCCAGCGGCGCATTCGTATTACTATCGTACATGAGCCCACAACCGAGATGAAGTGGAAGGACATCAATGAGTTGGTGG
TTGGACGTATCCGCAATACACCGGAGTCATCCGACGAACAGGACGAAGACGCCTGTGTCTTATCTTTGGGCTTGTTCCCAGGCGAGGCTT
TGGAGGTGCCCGGAGATGATAGATCTTTCTACCGTTTTGAGGCTGCCTGGGACTCGAGTCTGCACAACTCGGCCACTGCTCAAGAAGGA
ACGAAATCTTGGTCTCGCACTGCACGCGGGAAAC

parental A1405V

ATGTACCAGCTCTACTTATGTGCGCGGCGAGTCAGAATCTTCATGGCTGGAGGCCAAGGGGTGACTCCCTGATCTTCGATCACCAGTGG
GAGCTGGAGAAACTCACCAGACTTGAAGAGGTTGGACGCATGCGGCACTTGCTTCTGCTGCGCGAACGTCTGGGCATGGACACCAACCC
GAATCCGACCACCAAGACCGAGAAGGATGTTTGCAATCTAGCTGCTCGGGCAGTCACATCACCCGTACATATGGTCATTCCACAATCGCC
GCAGACTCCGGTCAAGGACCCACAGCAAATCATTCCAGAACGCGAGTACAACCAACGGGAGCAGGATCTCATGCTTAAATGCTTAAAAT
TGGTGCAGGGTGAGTTAATACTGAGACTTACCAAGCGTTCCATTCACTCTATTCTAAATTCATTTAAGGACGCTATACTAAGAGCGAGGC
CAACGATACGCAAACTCAGTCGGATGTTTCGCCTAGCGATGAGGGATGTGCCGATATGACCGTCAGCTGCATCTCCAGCAATTCCATGGA
GTGAGTAGTCGTTTAGCCACCCGTATAAACACACCACCCACACCAGCACCACCCATCTTAGTTAGCTGGACTCCCCCTTCCGCAAACCTTC
CTTAAATCCGGGTTTAGGGGCGAAAACCATCCAAACTGATTTGCGAACGTGGCTCCTCTTAGTAGGGCTTAA

Table S1 Statistical tests used in this study

Figure: 2E

Number:	Genotype:	n:
1	w^{1118};; **(WT)**	5
2	;*unc-104*^{bris}/*unc-104*^{bris} **(*unc-104*^{bris})**	6

Test: Student's two-tailed t-test

p-Value:

	1
1	
2	n.s.

Figure: 2F

Number:	Genotype:	n:
1	*elav*^{C155}*-Gal4 /+; ;UAS-unc-104*^{mCherry}/+ **(control)**	9
2	;*unc-104*^{bris}/*unc-104*^{d11024};*UAS-unc-104*^{mCherry}/+ **(*unc-104*^{bris}/-)**	10
3	*elav*^{C155}*-Gal4/+;unc-104*^{bris}/*unc-104*^{d11024};*UAS-unc-104*^{mCherry}/+ **(rescue)**	9

Test: One-Way ANOVA followed by Tukey's Multiple Comparison test

p-Value:

	1	2	3
1		***	n.s.
2			***
3			

Figure: 4A

Number:	Genotype:	n:
1	w^{1118};; **(WT)**	6
2	;*unc-104*^{bris}/*unc-104*^{bris} **(*unc*^{bris})**	8
3	;*unc-104*^{bris}/*unc-104*^{d11024} **(*unc-104*^{bris}/-)**	8
4	*elavX-Gal4 /+; ;UAS-unc-104*^{mCherry}/+ **(control)**	6
5	*elavX-Gal4 /+;unc-104*^{bris}/*unc-104*^{d11024} ;*UAS-unc-104*^{mCherry}/+ **(rescue)**	6

Test: One-Way ANOVA followed by Tukey's Multiple Comparison test

p-Value:

	1
1	
2	***
3	***
4	n.s.
5	n.s.

1-2.5 mm

	1
1	
2	***
3	***
4	n.s.
5	n.s.

2.6-4 mm

Figure: **6C**

Number:	**Genotype:**	**n:**
1	*elav ^{C155}-Gal4 /+; ;UAS-unc-104 ^{mCherry}/+* **(control)**	9
2	*;unc-104 ^{bris} /unc-104 ^{d11024};UAS-unc-104 ^{mCherry}/+* **(*unc-104 ^{bris}*/-)**	10
3	*elav ^{C155}-Gal4/+;unc-104 ^{bris} /unc-104 ^{d11024};UAS-unc-104 ^{mCherry}/+* **(rescue)**	9

Test: Kruskal-Wallis H-test followed by Mann-Whitney pairwise comparison test

p-Value: (Bonferroni corrected)

	1	**2**	**3**
1		***	**n.s.**
2			**
3			

Figure: **6D**

Number:	**Genotype:**	**n:**
1	*elav ^{C155}-Gal4 /+; ;UAS-unc-104 ^{mCherry}/+* **(control)**	9
2	*;unc-104 ^{bris} /unc-104 ^{d11024};UAS-unc-104 ^{mCherry}/+* **(*unc-104 ^{bris}*/-)**	10
3	*elav ^{C155}-Gal4/+;unc-104 ^{bris} /unc-104 ^{d11024};UAS-unc-104 ^{mCherry}/+* **(rescue)**	9

Test: Kruskal-Wallis H-test followed by Mann-Whitney pairwise comparison test

p-Value: (Bonferroni corrected)

	1	**2**	**3**
1		**	**n.s.**
2			*
3			

Figure: **7B**

Number:	**Genotype:**	**n:**
1	*elav ^{C155}-Gal4 /+;;* **(control)**	9
2	*elav ^{C155}-Gal4 /+;unc-104 ^{bris} /unc-104 ^{d11024}* **(*unc-104 ^{bris}*/-)**	8
3	*elav ^{C155}-Gal4 /+;unc-104 ^{bris} /unc-104 ^{d11024};UAS-Brp* **(unc-104^{bris}/-; Brp↑)**	8

Test: Kruskal-Wallis H-test followed by Mann-Whitney pairwise comparison test

p-Value: (Bonferroni corrected)

	1	**2**	**3**
1		*	**n.s.**
2			**
3			

Figure: **7C**

Number:	**Genotype:**	**n:**
1	*elav ^{C155}-Gal4 /+;;* **(control)**	9
2	*elav ^{C155}-Gal4 /+;unc-104 ^{bris} /unc-104 ^{d11024}* **(*unc-104 ^{bris} /-*)**	8
3	*elav ^{C155}-Gal4 /+;unc-104 ^{bris} /unc-104 ^{d11024} ;UAS-Brp/+* **(*unc-104 ^{bris} /-; Brp ↑*)**	8

Test: Kruskal-Wallis H-test followed by Mann-Whitney pairwise comparison test

p-Value: (Bonferroni corrected)

	1	**2**	**3**
1		**	n.s.
2			**
3			

Figure: **7D**

Number:	**Genotype:**	**n:**
1	*elav ^{C155}-Gal4 /+;;* **(control)**	9
2	*elav ^{C155}-Gal4 /+;unc-104 ^{bris} /unc-104 ^{d11024}* **(*unc-104 ^{bris} /-*)**	8
3	*elav ^{C155}-Gal4 /+;unc-104 ^{bris} /unc-104 ^{d11024} ;UAS-Brp/+* **(*unc-104 ^{bris} /-; Brp ↑*)**	8

Test: Kruskal-Wallis H-test followed by Mann-Whitney pairwise comparison test

p-Value: (Bonferroni corrected)

	1	**2**	**3**
1		**	**
2			*
3			

Figure: **8B**

Number:	**Genotype:**	**n:**
1	*w ^{1118} ;;* **(WT)**	7
2	*;unc-104 ^{bris} /+* **(*unc-104 ^{bris} /+*)**	9
3	*;unc-104 ^{bris} /unc-104 ^{bris}* **(*unc-104 ^{bris}*)**	7
4	*;unc-104 ^{bris} /unc-104 ^{d11024}* **(*unc-104 ^{bris} /-*)**	9

Test: Kruskal-Wallis H-test followed by Mann-Whitney pairwise comparison test

p-Value: (Bonferroni corrected)

	1	**2**	**3**	**4**
1		n.s.	*	**
2			n.s.	**
3				n.s.
4				

Figure: **8C**

Number:	**Genotype:**	**n:**
1	w^{1118};; **(WT)**	7
2	;*unc-104*^{bris}/+ **(*unc-104*^{bris}/+)**	9
3	;*unc-104*^{bris}/*unc-104*^{bris} **(*unc-104*^{bris})**	7
4	;*unc-104*^{bris}/*unc-104*^{d11024} **(*unc-104*^{bris}/-)**	9

Test: Kruskal-Wallis H-test followed by Mann-Whitney pairwise comparison test

p-Value: (Bonferroni corrected)

	1	**2**	**3**	**4**
1		**n.s.**	**n.s.**	**n.s.**
2			**n.s.**	**n.s.**
3				**n.s.**
4				

Figure: **8D**

Number:	**Genotype:**	**n:**
1	w^{1118};; **(WT)**	7
2	;*unc-104*^{bris}/+ **(*unc-104*^{bris}/+)**	9
3	;*unc-104*^{bris}/*unc-104*^{bris} **(*unc-104*^{bris})**	7
4	;*unc-104*^{bris}/*unc-104*^{d11024} **(*unc-104*^{bris}/-)**	9

Test: Kruskal-Wallis H-test followed by Mann-Whitney pairwise comparison test

p-Value: (Bonferroni corrected)

	1	**2**	**3**	**4**
1		**n.s.**	*	**
2			*	*
3				**n.s.**
4				

Figure: **8F**

Number:	**Genotype:**	**n:**
1	w^{1118};; **(WT)**	8
2	;*unc-104*^{bris}/+ **(*unc-104*^{bris}/+)**	10
3	;*unc-104*^{bris}/*unc-104*^{bris} **(*unc-104*^{bris})**	10
4	;*unc-104*^{bris}/*unc-104*^{d11024} **(*unc-104*^{bris}/-)**	10

Test: One-Way ANOVA followed by Tukey's Multiple Comparison test

p-Value: (Bonferroni corrected)

	1	**2**	**3**	**4**
1		***	***	***
2			***	***
3				**n.s.**
4				

Figure: **8G**

Number:	**Genotype:**	**n:**
1	w^{1118};; **(WT)**	8
2	;*unc-104*^{bris}/+ **(*unc-104*^{bris}/+)**	10
3	;*unc-104*^{bris}/*unc-104*^{bris} **(*unc-104*^{bris})**	10
4	;*unc-104*^{bris}/*unc-104*^{d11024} **(*unc-104*^{bris}/-)**	10

Test: One-Way ANOVA followed by Tukey's Multiple Comparison test

p-Value: (Bonferroni corrected)

	1	**2**	**3**	**4**
1		**	***	***
2			***	***
3				**n.s.**
4				

Figure: **8I**

Number:	**Genotype:**	**n:**
1	w^{1118};; **(WT)**	10
2	;*unc-104*^{bris}/+ **(*unc-104*^{bris}/+)**	10
3	;*unc-104*^{bris}/*unc-104*^{bris} **(*unc-104*^{bris})**	10
4	;*unc-104*^{bris}/*unc-104*^{d11024} **(*unc-104*^{bris}/-)**	10

Test: Kruskal-Wallis H-test followed by Mann-Whitney pairwise comparison test

p-Value: (Bonferroni corrected)

	1	**2**	**3**	**4**
1		**n.s.**	**	**
2			**	**
3				**
4				

Figure: **8J**

Number:	**Genotype:**	**n:**
1	w^{1118};; **(WT)**	10
2	;*unc-104*^{bris}/+ **(*unc-104*^{bris}/+)**	10
3	;*unc-104*^{bris}/*unc-104*^{bris} **(*unc-104*^{bris})**	10
4	;*unc-104*^{bris}/*unc-104*^{d11024} **(*unc-104*^{bris}/-)**	10

Test: Kruskal-Wallis H-test followed by Mann-Whitney pairwise comparison test

p-Value: (Bonferroni corrected)

	1	**2**	**3**	**4**
1		**n.s.**	*	*
2			**n.s.**	*
3				**n.s.**
4				

Figure: **8K**

Number:	Genotype:	n:
1	*w*^{1118}*;;* **(WT)**	8
2	*;unc-104*^{bris}*/+* **(*unc-104*^{bris}*/+*)**	10
3	*;unc-104*^{bris}*/unc-104*^{bris} **(*unc-104*^{bris})**	10
4	*;unc-104*^{bris}*/unc-104*^{d11024} **(*unc-104*^{bris}*/-*)**	10

Test: Kruskal-Wallis H-test followed by Dunn's Multiple Comparison test

p-Value:

	1	2	3	4
1		n.s.	*	***
2			*	***
3				n.s.
4				

Figure: **9B**

Number:	Genotype:	n:
1	*elav*^{C155}*-Gal4 /+; ;UAS-unc-104*^{mCherry}*/+* **(control)**	9
2	*;unc-104*^{bris}*/unc-104*^{d11024}*;UAS-unc-104*^{mCherry}*/+* **(*unc-104*^{bris}*/-*)**	11
3	*elav*^{C155}*-Gal4/+;unc-104*^{bris}*/unc-104*^{d11024}*;UAS-unc-104*^{mCherry}*/+* **(rescue)**	8

Test: Kruskal-Wallis H-test followed by Mann-Whitney pairwise comparison test

p-Value: (Bonferroni corrected)

	1	2	3
1		**	n.s.
2			**
3			

Figure: **9C**

Number:	Genotype:	n:
1	*elav*^{C155}*-Gal4 /+; ;UAS-unc-104*^{mCherry}*/+* **(control)**	9
2	*;unc-104*^{bris}*/unc-104*^{d11024}*;UAS-unc-104*^{mCherry}*/+* **(*unc-104*^{bris}*/-*)**	11
3	*elav*^{C155}*-Gal4/+;unc-104*^{bris}*/unc-104*^{d11024}*;UAS-unc-104*^{mCherry}*/+* **(rescue)**	8

Test: Kruskal-Wallis H-test followed by Mann-Whitney pairwise comparison test

p-Value: (Bonferroni corrected)

	1	2	3
1		n.s.	n.s.
2			n.s.
3			

Figure: **9D**

Number:	Genotype:	n:
1	*elav ^{C155}-Gal4 /+; ;UAS-unc-104 ^{mCherry}/+* **(control)**	9
2	*;unc-104 ^{bris} /unc-104 ^{d11024};UAS-unc-104 ^{mCherry}/+* **(*unc-104 ^{bris}*/-)**	11
3	*elav ^{C155}-Gal4/+;unc-104 ^{bris} /unc-104 ^{d11024};UAS-unc-104 ^{mCherry}/+* **(rescue)**	8

Test: Kruskal-Wallis H-test followed by Mann-Whitney pairwise comparison test

p-Value: (Bonferroni corrected)

	1	2	3
1		**	n.s.
2			**
3			

Figure: **9F**

Number:	Genotype:	n:
1	*elav ^{C155}-Gal4 /+; ;UAS-unc-104 ^{mCherry}/+* **(control)**	9
2	*;unc-104 ^{bris} /unc-104 ^{d11024};UAS-unc-104 ^{mCherry}/+* **(*unc-104 ^{bris}*/-)**	10
3	*elav ^{C155}-Gal4/+;unc-104 ^{bris} /unc-104 ^{d11024};UAS-unc-104 ^{mCherry}/+* **(rescue)**	9

Test: One-Way ANOVA followed by Tukey's Multiple Comparison test

p-Value:

	1	2	3
1		***	n.s.
2			***
3			

Figure: **9G**

Number:	Genotype:	n:
1	*elav ^{C155}-Gal4 /+; ;UAS-unc-104 ^{mCherry}/+* **(control)**	9
2	*;unc-104 ^{bris} /unc-104 ^{d11024};UAS-unc-104 ^{mCherry}/+* **(*unc-104 ^{bris}*/-)**	10
3	*elav ^{C155}-Gal4/+;unc-104 ^{bris} /unc-104 ^{d11024};UAS-unc-104 ^{mCherry}/+* **(rescue)**	9

Test: One-Way ANOVA followed by Tukey's Multiple Comparison test

p-Value:

	1	2	3
1		***	n.s.
2			***
3			

Figure: **11B**

Number:	Genotype:	n:
1	*elav^{C155}-Gal4 /+;unc-104^{bris}/unc-104^{d11024}* (***unc-104^{bris}/-***)	8
2	*elav^{C155}-Gal4 /+;unc-104^{bris}/unc-104$^{d11024;}$ UAS-Brp-RNAi* (***Brp↓***)	8
3	*elav^{C155}-Gal4 /+;unc-104^{bris}/unc-104$^{d11024;}$ UAS-Brp* (***Brp↑***)	8

Test: One-Way ANOVA followed by Tukey's Multiple Comparison test

p-Value:

	1	2	3
1		n.s.	n.s.
2			n.s.
3			

Figure: **11C**

Number:	Genotype:	n:
1	*elav^{C155}-Gal4 /+;unc-104^{bris}/unc-104^{d11024}* (***unc-104^{bris}/-***)	8
2	*elav^{C155}-Gal4 /+;unc-104^{bris}/unc-104$^{d11024;}$ UAS-Brp-RNAi* (***Brp↓***)	8
3	*elav^{C155}-Gal4 /+;unc-104^{bris}/unc-104$^{d11024;}$ UAS-Brp* (***Brp↑***)	8

Test: One-Way ANOVA followed by Tukey's Multiple Comparison test

p-Value:

	1	2	3
1		n.s.	n.s.
2			n.s.
3			

Figure: **11D**

Number:	Genotype:	n:
1	*elav^{C155}-Gal4 /+;unc-104^{bris}/unc-104^{d11024}* (***unc-104^{bris}/-***)	8
2	*elav^{C155}-Gal4 /+;unc-104^{bris}/unc-104$^{d11024;}$ UAS-Brp-RNAi* (***Brp↓***)	8
3	*elav^{C155}-Gal4 /+;unc-104^{bris}/unc-104$^{d11024;}$ UAS-Brp* (***Brp↑***)	8

Test: One-Way ANOVA followed by Tukey's Multiple Comparison test

p-Value:

	1	2	3
1		n.s.	n.s.
2			n.s.
3			

Figure: **11E**

Number:	Genotype:	n:
1	*elav^{C155}-Gal4 /+;unc-104^{bris}/unc-104^{d11024}* **(*unc-104^{bris}/-*)**	8
2	*elav^{C155}-Gal4 /+;unc-104^{bris}/unc-104$^{d11024;}$ UAS-Brp-RNAi* **(*Brp*↓)**	8
3	*elav^{C155}-Gal4 /+;unc-104^{bris}/unc-104$^{d11024;}$ UAS-Brp* **(*Brp*↑)**	8

Test: One-Way ANOVA followed by Tukey's Multiple Comparison test

p-Value:

	1	2	3
1		n.s.	n.s.
2			n.s.
3			

Figure: **11F**

Number:	Genotype:	n:
1	*elav^{C155}-Gal4 /+;unc-104^{bris}/unc-104^{d11024}* **(*unc-104^{bris}/-*)**	8
2	*elav^{C155}-Gal4 /+;unc-104^{bris}/unc-104$^{d11024;}$ UAS-Brp-RNAi* **(*Brp*↓)**	8
3	*elav^{C155}-Gal4 /+;unc-104^{bris}/unc-104$^{d11024;}$ UAS-Brp* **(*Brp*↑)**	8

Test: One-Way ANOVA followed by Tukey's Multiple Comparison test

p-Value:

	1	2	3
1		n.s.	n.s.
2			n.s.
3			